# Evaluation of iceberg calving models against observations from Greenland outlet glaciers

A Thesis

Presented in Partial Fulfillment of the Requirements for the

Degree of Master of Science

with a

Major in Geology

in the

College of Graduate Studies

University of Idaho

by

Tristan O. Amaral

Major Professor: Timothy C. Bartholomaus, Ph.D.

Committee Members: Ellyn M. Enderlin, Ph.D., Eric Mittelstaedt, Ph.D.

Department Chair: Leslie Baker, Ph.D.

May 2019

**Authorization to Submit Thesis**

This thesis of Tristan O. Amaral, submitted for the degree of Master of Science with a Major in Geology and titled "Evaluation of iceberg calving models against observations from Greenland outlet glaciers," has been reviewed in final form. Permission, as indicated by the signatures and dates below, is now granted to submit final copies to the College of Graduate Studies for approval.

Major Professor: _____ Date:_____
Timothy C. Bartholomaus, Ph.D.

Committee Members: _____ Date:_____
Ellyn M. Enderlin, Ph.D.

_____ Date:_____
Eric Mittelstaedt, Ph.D.

Department
Chair: _____ Date:_____
Leslie Baker, Ph.D.

## Abstract

The retreat and advance of marine-terminating outlet glaciers in Greenland plays a critical role in modulating ice sheet mass balance. However, the frontal ablation processes that regulate glacier terminus positions are challenging to observe and thus difficult to represent in numerical ice flow models. Current models of the Greenland Ice Sheet rely upon simple iceberg calving and submarine melt parameterizations to prescribe either a stable terminus position or iceberg calving rate, yet the relative accuracies and uncertainties of these criteria remain largely unknown at the ice sheet scale. Here, we evaluate six iceberg calving models from the literature against spatially and temporally diverse observations and model output from 50 marine-terminating outlet glaciers in Greenland. Five of six calving models successfully reproduce observed May/June terminus conditions with zero median model bias and low ice-sheet-wide uncertainty using fixed, spatially-optimized parameter values. However, when evaluated against time series observations from select glaciers, we find that calving models that predict a calving rate struggle to reproduce variations in observed terminus dynamics over seasonal and inter-annual time scales with single, optimized model parameters. Comparatively, calving models that prescribe a terminus position, rather than a calving rate, more accurately account for observed changes in terminus dynamics through time and are therefore less likely to generate glacier length and/or ice flux errors when employed in predictive ice flow models. Overall, our results indicate that the crevasse depth calving model reproduces observed terminus dynamics with high fidelity and should be considered a leading candidate for use in models of the Greenland Ice Sheet.

**Acknowledgements**

This work represents a culmination of academic mentorship, inspiration, and support that began well before my arrival at the University of Idaho. In particular, I extend appreciation to Dr. Cameron P. Wake at the University of New Hampshire, and Dr. Shad O'Neel at the USGS Alaska Science Center for guidance and recommendations on graduate school. I owe much of my fascination with glaciology and motivation to pursue research to the Juneau Icefield Research Program and the community of scientists involved with the program.

My committee members, Dr. Eric Mittelstaedt from the University of Idaho and Dr. Ellyn M. Enderlin from Boise State University, deserve acknowledgement for insightful discussions during the research process and helpful reviews that steered this thesis in the right direction.

Lastly, my advisor, Dr. Timothy C. Bartholomaus at the University of Idaho, deserves supreme thanks for his time and effort spent helping me through the graduate research process. It was a privilege to work with someone who embodies such creativity, optimism, and genuine eagerness to continue learning.

Funding for this work was in part provided by grant number NNX17AJ99G from the NASA Goddard Space Flight Center awarded to Dr. Timothy C. Bartholomaus.

## Dedications

This thesis is dedicated to the friends and family that made graduate school a successful experience. To my parents, for their unwavering support in my life choices, and for predisposing me to the natural sciences at a young age. And to my friends in the University of Idaho graduate student community who truly value a healthy balance and infused my two years with more humor, friendship, and support than I could have asked for.

## Table of Contents

## List of Tables

## List of Figures

## 1. Introduction

Since 1993, sea level rise contribution from the Greenland Ice Sheet has increased eightfold from ~0.1 mm/yr to ~0.8 mm/yr and presently accounts for over one fifth of observed global mean sea level rise (Csatho et al., 2014; Chen et al., 2017, Dieng et al., 2017). Between one-third and one-half of Greenland's ice mass loss are attributed to dynamic ice discharge from marine-terminating outlet glaciers that drain the ice sheet (Enderlin et al., 2014; Van den Broeke et al., 2016; King et al., 2018). Dynamic discharge has increased substantially over the past two decades and is projected to remain a significant contributor to Greenland's Ice Sheet mass flux on decadal time scales in the future (Morlighem et al., 2017, 2019; Aschwanden et al., in review). Changes to dynamic discharge arise at the ice/ocean boundary, where abrupt outlet glacier retreat triggers accelerated ice flow and upstream thinning (Nick et al., 2009; Murray et al., 2010; Rignot et al., 2010). Accurate predictions of dynamic discharge from the Greenland Ice Sheet therefore hinge on realistic simulation of glacier terminus position of marine-terminating outlet glaciers (Vieli and Nick, 2011).

Outlet glacier terminus position is controlled by the processes of iceberg calving and submarine melt, together referred to as frontal ablation, which erode ice from the glacier front and balance glacier flow (Truffer and Motyka, 2016; Benn et al., 2017). Iceberg calving, the mechanical removal of ice from a glacier terminus, ultimately results from fracture when stresses at the glacier front exceed ice strength. Relevant stresses include extensional stresses associated with ice flow near the glacier terminus, torque arising from buoyancy forces, backpressure from ice mélange, force imbalance at the ice cliff, and melt undercutting of the calving front (van der Veen, 1996; Benn et al., 2007a; Bassis and Jacobs, 2013). Observations of disparate iceberg calving styles suggest that the relative contributions of these controlling parameters vary tremendously: glaciers featuring large floating ice tongues such as in northern Greenland or Antarctica will infrequently calve enormous shelves of ice (Falkner et al., 2011), while several of Greenland's largest outlet glaciers featuring lightly grounded termini, such as Helheim Glacier, are dominated by full-thickness, buoyancy-driven calving events (Veitch and Nettles, 2012; James et al., 2014). Still smaller, grounded glaciers found in Greenland or Alaska have been observed to calve hundreds of 10-100 m scale ice chunks in a single day (Bartholomaus et al., 2012; Fried et al., 2018). Submarine melting of glacier termini is a result of heat transfer from ocean waters to submerged ice, a process that is

largely controlled by subglacial runoff flux, ocean water temperatures and salinity, and terminus morphology (Jenkins, 2011; Truffer and Motyka, 2016). Estimates of submarine melting on marine-terminating glaciers exhibit variability that mirrors that found for calving: polar glaciers abutting cold ocean waters in Northern Greenland and Antarctica feature melt rates on the order of 1-10 m per year when averaged over the subaqueous face (Enderlin and Howat, 2013; Rignot et al., 2013) whereas at faster, more temperate glaciers in Greenland and Alaska submarine melting can conceivably erode more than 10 m of ice in a single day (Bartholomaus et al., 2013; Motyka et al., 2013; Fried et al., 2015; Rignot et al., 2016a). Furthermore, submarine melting and iceberg calving are not necessarily independent processes, though currently the relationship between the two processes remains largely unconstrained (e.g., O'Leary and Christoffersen, 2013; Cook et al., 2014). Observations from Svalbard, Norway have led some to hypothesize that submarine melting enhances, or even paces, the process of iceberg calving through undercutting of the terminus ice cliff (Luckman et al., 2015), while observations from Greenland outlet glaciers suggest that the relative contributions of melting and calving are highly variable from glacier to glacier (Enderlin and Howat, 2013; Rignot et al., 2016b; Wood et al., 2018).

The physical complexity and observed variability in iceberg calving and submarine melting processes complicates the inclusion of frontal ablation in numerical glacier models. Despite concerted effort over the last decade, a universal numerical representation of frontal ablation for marine-terminating glaciers has eluded scientific consensus (James et al., 2014; Benn et al., 2017). More than a dozen parameterizations and frameworks have been put forth to accommodate varying mechanisms for iceberg calving and submarine melting in different glaciated regions that employ both theoretical and empirical means. These parameterizations include calving models (also known as *calving laws*), submarine melting models, and coupled calving/melting models that all formulate either a stable terminus position or an ablation rate. Most frontal ablation criteria represent terminus dynamics only in terms of iceberg calving (van der Veen; Benn et al., 2007b; Bassis and Walker, 2012; Levermann et al., 2012; Mercenier et al., 2017), due in part to historic under-appreciation of submarine melting rates (Truffer and Motyka, 2016). More recently, attempts have been made to incorporate both iceberg calving and submarine melting into frontal ablation criteria for numerical glacier models (Morlighem et al., 2016, Todd et al., 2018) and even to formulate frontal ablation

exclusively as a function of submarine undercutting (Luckman et al., 2015). Another approach to frontal ablation modeling utilizes discrete-element models to simulate individual calving events (Bassis and Jacobs, 2013; Astrom et al., 2014). Although these models generate highly realistic calving events across a wide spectrum of calving styles, their high computation demands currently precludes their use in prognostic glacier flow models (Benn et al., 2017).

Current models of the Greenland Ice Sheet rely upon simple frontal ablation equations as boundary criteria to represent advance and retreat of the ice sheet marine boundary (Benn et al., 2017). The choice of terminus boundary criteria in existing ice sheet models varies from fixed glacier extents or simple flotation thresholds to more sophisticated representations of both calving and submarine melting processes (Goelzer et al., 2018). The lack of consensus amongst ice sheet models on which terminus boundary criteria should be employed in part reflects the fact that the relative accuracies of existing frontal ablation criteria are largely unconstrained. Inaccurate representation of terminus dynamics will result in inaccurate perturbations to the force balance that governs ice flow, which may at least partially explain the large disparity between dynamic discharge predictions by different ice sheet models (Furst et al., 2015; Aschwanden et al., 2016; Peano et al., 2017). Inversely, accurate simulation of terminus dynamics improves modeled mass flux estimates, as recently demonstrated by Haubner et al. (2018). When input with historical terminus positions, Haubner et al. (2018) found that the Ice Sheet System Model (ISSM) was able to reproduce past mass flux at Upernavik Isstrom in Greenland with high fidelity to observed estimates. It is therefore expected that the incorporation of improved frontal ablation criteria into prognostic ice sheet models will increase confidence in projections of dynamic discharge from Greenland.

To date, frontal ablation model generation has outpaced comprehensive validation of existing models and thus relative model accuracies and uncertainties remain largely unquantified at the ice sheet scale (Benn et al., 2017). Each published frontal ablation model has successfully reproduced elements of terminus dynamics at either observed or idealized glacier settings, but methods of validation vary considerably amongst models. Some frontal ablation criteria have been validated against observational data sets consisting of measurements from several tidewater glaciers (van der Veen, 1996; Vieli et al., 2001; Bassis and Walker, 2012; Levermann et al., 2012, Mercenier et al., 2017) while others have been

evaluated via implementation in 1-D, 2-D, or 3-D ice flow models (Nick et al., 2010; Otero et al., 2010; Morlighem et al., 2016, Todd et al., 2018). Process-driven ice flow models test calving models via qualitative comparison of modeled terminus change with observed terminus behavior (e.g., Cook et al., 2012), however, ice flow parameters such as basal traction, ice rheology, and surface mass balance often carry unknown uncertainties which impact modeled terminus dynamics in ways similar to the terminus boundary condition (e.g., Benn et al., 2007b. Recent evaluations of the same calving criteria by two different ice flow models (Choi et al., 2018; Todd et al., 2018) resulted in dissimilar assessments of calving performance, suggesting that the choice of ice flow model impacts the performance of the calving model under investigation. The use of observational data to evaluate frontal ablation criteria avoids the unquantified influence of other model components by allowing the frontal ablation criterion to be tested in isolation. However, none of the existing frontal ablation models have been validated at the ice sheet scale using consistent datasets and methods. There is thus is a need for a thorough, observational evaluation of frontal ablation criteria to resolve the relative accuracies and uncertainties of these criteria at the ice-sheet scale.

The recent proliferation of ice velocity observations (e.g., Howat, 2017), ice elevation measurements (e.g., Porter et al., 2018) and improved bed elevation estimates (Morlighem et al., 2017) across Greenland enables examination of terminus dynamics in greater detail than was possible even several years ago. In this paper, we use observational and modeled data from Greenland to thoroughly evaluate and inter-compare six calving models. These six calving models are either currently employed or are candidates for use in ice sheet models of the Greenland Ice Sheet (Goelzer et al., 2018). Using observations from a diverse and representative sample of 50 outlet glaciers encircling the ice sheet, we empirically calibrate the free parameter in each calving model by identifying the parameter value that minimizes the misfit between predicted and observed calving behaviors. We perform three calibration tests: First, we calibrate the six calving models to individual glaciers to examine spatial variability in optimal model parameters and to reveal the range of calibrated parameters needed for each model to reproduce observed terminus conditions across 50 sample glaciers. Second, we test the ability of the six calving models to account for spatial variability in frontal ablation using a single model configuration that is calibrated to the 50 sample glaciers as a whole. This test provides measures of ice-sheet-wide misfit between modeled and observed

calving quantities, which allows us to quantify the relative accuracy and uncertainty associated with each calving model at the ice sheet scale. Lastly, we investigate the temporal dependence of model calibration using temporally-dense observations from four of the 50 outlet glaciers. Based on these three analyses, we make recommendations regarding the use of calving models as boundary criteria for Greenland Ice Sheet model simulations and identify patterns of calving model shortcomings that require improvement.

## 2. Data and Methods

### 2.1 Frontal Ablation Models

| (Abbr.) | Calving Model Name | Numerical Formula | Citation |
|---|---|---|---|
| (HAF) | Height Above Flotation | $H \geq H_b + h_c$ | van Der Veen, 1996 |
| (FAF) | Fraction Above Flotation | $H \geq H_b(1+f)$ | Vieli et al., 2001 |
| (CD) | Crevasse Depth | $h > d_s, H > d_s + d_b$ | |
| | - Surface crevasses | $d_s = \frac{R_{xx}}{\rho_i g} + \frac{\rho_w}{\rho_i} d_w$ | Benn et al., 2007 |
| | - Basal crevasses | $d_{bcrev} = \frac{\rho_i}{\rho_{sw} - \rho_i}\left[\frac{R_{xx}}{\rho_i g} - (H_{ab})\right]$ | Nick et al., 2010 |
| (VM) | von Mises | $u_c = \|v\| \frac{\sqrt{3} B \dot{\varepsilon}_{te}^{\left(\frac{1}{n}\right)}}{\sigma_{max}}$ | Morlighem et al., 2016 |
| (SR) | Stress Relation | $u_c = \frac{x_m H}{T_f} = \tilde{B}(1-\omega^{2.8}) \cdot \left(\sigma_{1,m} - \sigma_{th}\right)^r H$ | Mercenier et al., 2017 |
| (EC) | Eigencalving | $u_c = K \cdot \max(\dot{\varepsilon}_1, 0) \cdot \max(\dot{\varepsilon}_2, 0)$ | Levermann et al., 2012 |

Table 2.1: Six iceberg calving model formulations validated in this study. Each model estimates glacier terminus position in terms of either ice stability criteria or rate of calving. Models 1-3 predict the calving margin will retreat to where the ice thickness inequality is satisfied. Models 4-6 formulate calving as a calving rate, $u_c$. Full parameter definitions are provided in table 2.2 and in text. Note: models are herein referred to in the text according to abbreviation listed in parentheses to left of model name.

We select six frontal ablation criteria from the literature to evaluate against observations from Greenland outlet glaciers (Table 2.1). Three of the criteria represent the balance of frontal ablation and ice velocity as a modeled terminus position (herein: *calving position models*) while the other three criteria represent frontal ice loss as a modeled frontal ablation rate (herein: *calving rate models*). The calving position models include two buoyancy-based terminus criteria – Height above flotation (HAF; van der Veen, 1996) and Fraction above Flotation (FAF; Vieli et al., 2001) – and a crevasse-depth criterion (CD; Benn et al., 2007b; Nick et al., 2010). In both the HAF and FAF models, the buoyancy of the glacier exerts a first-order control on the location of the calving front. The glacier terminus is permitted to thin until it reaches a critical height-above-buoyancy, whereupon ice is predicted to calve off. In the HAF model, the critical ice thickness is the sum of the buoyancy height and a fixed height, $h_c$, such that the ice thickness must satisfy the inequality,

$$H \geq H_b + h_c \,, \tag{1}$$

where $H_b = \frac{\rho_{sw}}{\rho_i} D$, taking $D$ to be the fjord depth/negative of the glacier bottom elevation and $\rho_{sw}$ and $\rho_i$ are densities of sea water and ice, respectively. The FAF model parameterizes the height-above-buoyancy threshold as a fraction, *f*, of the water depth to account for observed differences in ice cliff height between thick, fast-flowing and thin, slow-flowing marine-terminating glaciers (Vieli et al., 2001):

$$H \geq H_b(1 + f). \tag{2}$$

Since there is no theoretical derivation for the values of $h_c$ and $f$, we treat them as free parameters that must be calibrated to observations. Although neither the HAF nor FAF model permit floating ice, the preponderance of grounded glaciers in Greenland and the continued use of flotation criteria in ice sheet models motivates the inclusion of these parameterizations in this study.

The CD frontal ablation model assumes that the first-order control on terminus position is longitudinal stretching in the large-scale velocity field near the glacier terminus (Benn et al., 2007b). In response to extensional stress, surface crevasses are assumed to penetrate to a depth where the longitudinal strain rate exactly balances the creep closure rate from ice overburden pressure (Nye, 1955; 1957),

$$d_s = \frac{\sigma}{\rho_i g}\,, \tag{3}$$

where $d_s$ is the depth of the crevasse and $\sigma$ is the tensile stress responsible for crevasse opening. Consistent with Nick et al. (2010), we represent $\sigma$ as the horizontal resistive stress, $R_{xx}$, which is defined as the full stress minus the lithostatic stress (van der Veen, 2013, pg 56). The value of $R_{xx}$ is calculated from observed strain rates using the constitutive equation (Glen, 1957), such that

$$R_{xx} = B\dot{\varepsilon}_e^{\frac{1-n}{n}}\,(2\dot{\varepsilon}_1 + \dot{\varepsilon}_2), \tag{4}$$

where $B$ and $n$ are the ice stiffness parameter and stress exponent, and $\dot{\varepsilon}_e$ is the effective strain rate defined as $\dot{\varepsilon}_e^2 = \frac{1}{2}(\dot{\varepsilon}_1^2 + \dot{\varepsilon}_2^2)$. Variables $\dot{\varepsilon}_1$ and $\dot{\varepsilon}_2$ are the two strain rate eigenvalues (corresponding to principle horizontal stress directions) that account for instances where the principle strain orientation is different from ice flow direction near the glacier terminus. The presence of water in surface crevasses deepens crevasse penetration depths through the added

downward pressure exerted by the water, $P_w = \rho_w g d_w$ (Benn et al., 2007b). The predicted depth of surface crevasses therefore becomes,

$$d_s = \frac{R_{xx}}{\rho_i g} + \frac{\rho_w}{\rho_i} d_w \,. \tag{5}$$

In addition, basal crevasses may form when a glacier is at or near flotation and longitudinal stretching rates are large. The propagation height of basal crevasses, $d_b$, may be estimated from $R_{xx}$ using a relation from Nick et al. (2010),

$$d_b = \frac{\rho_i}{\rho_{sw} - \rho_i}\left(\frac{R_{xx}}{\rho_i g} - H_{ab}\right), \tag{6}$$

where $H_{ab} = H - H_b$. Calving consequently occurs in the CD model where surface crevasses intersect the waterline, or where basal and surface crevasses intersect. The modelled glacier terminus is defined as the most seaward location where the following conditionals are both met,

$$h > d_s \,, \quad H > (d_s + d_b), \tag{7}$$

in which $h = H - D$. We treat the depth of the water in crevasses, $d_w$, as a free parameter, allowing the CD model to be calibrated empirically.

The three rate models include the eigencalving model (EC; Levermann et al., 2012), a von Mises criterion (VM) proposed by Morlighem et al. (2016), and a stress-based calving relation (SR) introduced by Mercenier et al. (2017). The eigencalving model predicts a calving rate proportional to the two strain rate eigenvalues near the glacier terminus,

$$u_c = K \cdot \max(\dot{\varepsilon}_1, 0) \cdot \max(\dot{\varepsilon}_2, 0) \,, \tag{8}$$

in which the eigenvalues are averaged over a stress coupling length near the terminus. The stress coupling length is calculated as 4.5 times the ice thickness, following empirical observations by Enderlin et al. (2016). Equation (8) implies that if either eigenvalue is compressional, calving is suppressed. The EC model relies upon the empirical proportionality constant, *K*, for calibration to observed calving rates (Levermann et al., 2012).

The VM criterion assumes that iceberg calving is governed by the tensile stress regime at the glacier terminus. Predicted calving rate depends on the ice velocity at the glacier terminus and is modified by the ratio of terminus tensile stress to a tensile stress threshold, $\sigma_{max}$,

$$u_c = v\frac{\sigma_{vm}}{\sigma_{max}}, \tag{9}$$

where the state of tensile stress at the terminus is given by the von Mises stress,

$$\sigma_{vm} = \sqrt{3} \cdot B \cdot \dot{\varepsilon}_{te}^{\frac{1}{n}}. \tag{10}$$

In equation 10, $\dot{\varepsilon}_{te}$ is the effective tensile strain rate, $\dot{\varepsilon}_{te}^2 = \frac{1}{2}[\max(\dot{\varepsilon}_1, 0) + \max(\dot{\varepsilon}_2, 0]$, averaged over the glacier stress coupling length nearest the terminus. When $\sigma_{vm} > \sigma_{max}$, the glacier will advance, and conversely, when $\sigma_{vm} < \sigma_{max}$ the glacier will retreat (Morlighem et al., 2016). At present there is no theoretical derivation for $\sigma_{max}$ so it is treated as a free parameter in the VM model. Note that the simple submarine melt parameterization that is coupled to the VM calving model in Morlighem et al. (2016) is left out of this study so that we may inter-compare the performance of the VM calving criterion directly to other calving rate parameterizations.

Calving in the SR model is primarily a function of the extensional stresses at the glacier termini resulting from the ice cliff imbalance (Mercenier et al., 2017). It is assumed that a large crevasse forms near the glacier terminus in response to the maximum principle stress (assuming tension is positive):

$$\sigma_1 = \rho_i g H(0.4 - 0.45(\omega - 0.065)^2). \tag{11}$$

The relative location ($x_m$) of the principle stress at the glacier surface is defined by its distance up-glacier from the terminus and is approximated in terms of the water depth and ice thickness,

$$x_m = 0.67(1 - \omega^{2.8}), \tag{12}$$

where $\omega = \frac{D}{H}$ and $x_m$ is a unitless fraction of the ice thickness. When full failure of the ice occurs at the location of $x_m$, it is assumed that the damaged ice is rapidly removed and $x_m$ becomes the location of the glacier terminus. Mercenier et al. (2017) propose that ice damage at $x_m$ may be accomplished through a variety of processes, including basal crevassing, hydro-fracturing via surface water, or rapid elastic crevasse propagation. The time needed for these processes to achieve ice failure is given according to the isotropic damage relation (Pralong et al., 2006),

$$T_f = \frac{(1 - D_0)^{r+k+1} - (1 - D_c)^{r+k+1}}{(r + k + 1)B_d(\sigma_1 - \sigma_{th})}, \tag{13}$$

in which $r$, $k$, and $B_d$ are damage constants, $D_0$ and $D_c$ are initial and critical damage values and $\sigma_{th}$ is the threshold stress that must be exceeded for damage initiation. Calving rate is thus expressed as a ratio of distance over time:

$$u_c = \frac{x_m H}{T_f} = \tilde{B}(1-\omega^{2.8}) \cdot \left(\sigma_{1,m} - \sigma_{th}\right)^r H. \quad (14)$$

In Equation 14, $\tilde{B}$ encompasses a constant term related to ice damage,

$$\tilde{B} = \left[\frac{0.67(r+k+1)B}{(1-D_0)^{r+k+1} - (1-D_c)^{r+k+1}}\right] = 65\ \mathrm{MPa^{-r}a^{-1}}. \quad (15)$$

A more complete explanation of variables is given in Mercenier et al. (2017). The SR model contains three empirical parameters: $\tilde{B}, r$, and $\sigma_{th}$ and is reported to not be very sensitive to the exact choice of parameter value within a reasonable range (Mercenier et al.,

| Variable/Parameter | Notation | Value/Range | Units | Model(s) |
|---|---|---|---|---|
| Ice thickness | H | | m | all |
| Ice surface elevation | h | | m | all |
| Water depth | D | | m | all |
| Ice surface velocity | v | | m $d^{-1}$ | VM |
| *Ice fraction above flotation | $f$ | 0 – 0.5 | | FAF |
| *Height above flotation | $h_c$ | 0 – 150 | m | HAF |
| Seawater density | $p_{sw}$ | 1020 | kg $m^{-3}$ | HAF,FAF,CD |
| Fresh water density | $p_w$ | 1000 | kg $m^{-3}$ | CD |
| Ice density | $p_i$ | 920 | kg $m^{-3}$ | HAF,FAF,CD |
| Gravitational acceleration | $g$ | 9.81 | m $s^{-2}$ | HAF,FAF,CD |
| Calving rate | $u_c$ | | m $d^{-1}$ | VM,SR,EC |
| Surface crevasse depth | $d_s$ | | m | CD |
| Basal crevasse depth | $d_b$ | | m | CD |
| *Crevasse water depth | $d_w$ | 0 – 150 | m | CD |
| Ice viscosity parameter | $B$ | 324 | kPa$^{-1}$ $yr^{-1/3}$ | CD,VM,EC |
| *Proportionality constant | $K$ | 1 – 500000 | m a | EC |
| Stress exponent | $n$ | 3 | | CD,VM |
| *Tensile stress threshold | $\sigma_{max}$ | 0.1 – 8.0 | MPa | VM |
| Effective strain rate | $\dot{\varepsilon}_e$ | | $d^{-1}$ | CD |
| Effective tensile strain rate | $\dot{\varepsilon}_{te}$ | | $d^{-1}$ | VM |
| First strain rate eigenvalue | $\dot{\varepsilon}_1$ | | $d^{-1}$ | CD,VM,EC |
| Second strain rate eigenvalue | $\dot{\varepsilon}_2$ | | $d^{-1}$ | CD,VM,EC |
| *Stress threshold for damage | $\sigma_{th}$ | 0.1 – 0.5 | MPa | SR |

Table 2.2: Model parameter names, notations, units, constant values or value testing ranges, and model involvement key. Asterisk (*) denotes free model parameters that are used to empirical calibrate models to observations.

2017). Therefore, we set $r = 0.5$, $\tilde{B} = 65$ MPa$^{-\mathrm{r}}$a$^{-1}$, and select $\sigma_{th}$ as our free parameter for model calibration since it features the simplest physical translation.

We endeavor here to evaluate many of the most well-known and broadly-applied frontal ablation models. However, our goal to test models against observations precludes the evaluation of several existing frontal ablation models for which we lack necessary environmental data of sufficient resolution or that which yield unrealistic results, notably the undercutting model by Luckman et al. (2015) and the yield strength criteria proposed by Bassis and Walker (2012). While models of submarine melt now exist (Xu et al., 2013; Rignot et al., 2016a, Slater et al., 2017), sufficient uncertainty in both the physical structure of these models and their uncertainties persist, such that we cannot be confident of their utility at ice sheet scale (Slater et al., 2018; Wagner et al., 2019). The six models tested in this study were designed only to represent mechanical calving processes and do not include explicit representation of submarine melting. However, since the six models are empirically calibrated to observations of total frontal ablation, submarine melting is implicitly accounted for in the resulting calibrated model configurations. Whilst it would be preferable to calibrate test the three calving rate models against direct measurements of calving rates alone and not frontal ablation rates, ice-sheet-wide partitioned calving rate estimates (as distinct from submarine melting) are presently unavailable for use in such a validation. Therefore, given the current state of submarine melt modeling and observations, we do not attempt to partition calving rates from observed frontal ablation rates. Instead, we rely upon implicit representation of submarine melting to model frontal ablation using a bulk, inclusive model, as is commonly done in ice sheet models (Goelzer et al., 2018).

### 2.2. Observational Data

The six calving models under investigation collectively rely on four fundamental data sets for variable inputs and model evaluation: bed elevation, ice surface elevation, ice surface velocity and observed terminus position. Using data from approximately one quarter of all marine-terminating outlet glaciers in Greenland, we test calving models on their ability to account for variability in glacier terminus change across a range of spatial and temporal scales.

Ice thickness data are derived from differencing ice elevation measurements obtained from NASA's Operation IceBridge Airborne Topographic Mapper (ATM) LiDAR and WorldView (WV) satellite stereo imagery with bed elevation estimates from Greenland BedMachine v3 (Morlighem et al., 2017). Operation IceBridge ATM observations provide ~250 m-wide swaths of ice elevation measurements recorded along glacier center profiles during April/May for all sample glaciers from 2009 to 2017. These elevation data have horizontal resolution of better than 1m and vertical accuracy of 0.07 cm (Martin et al., 2012). High resolution (2 m) DEMs constructed from DigitalGlobe's WV-1 and WV-2 satellite image pairs capture the lower ~5-10 km of outlet glaciers with approximately 3 m vertical uncertainty (Enderlin and Hamilton, 2014; Noh and Howat, 2015). BedMachine v3 combines radar-constrained mass conservation modeling with bathymetric measurements around the ice sheet periphery to create a seamless, 150 m resolution map of Greenland bed elevations (Morlighem et al., 2017; https://nsidc.org/data/IDBMG4). The accuracy of bed estimates near the termini of outlet glaciers sampled in this study is generally better than 50 m.

Ice surface velocities are extracted from speckle-tracking of satellite imagery from both optical (Howat et al., 2017) and radar (Joughin et al., 2010) sensors from NASA Making Earth System Data Records for Use in Research Environments (MEaSUREs) products (NSIDC; http://nsidc.org/data/nsidc-0481; http://nsidc.org/data/nsidc-0646). These 100 m resolution velocity maps capture the fast-flowing trunks and termini of Greenland outlet glaciers with systematic errors estimated at 3% of the velocity (Joughin et al., 2010). Ice velocity maps corresponding to each ice elevation profile or WV DEM are generally from within 45 days of the ice elevation observation, with 85% within 30 days. For ATM elevation measurements from late April and May, the corresponding ice velocities are all from May or June due to the absence of velocity maps during early spring. For the velocities corresponding to WV DEMs, 35% precede the data of elevation measurement while 65% succeed the elevation date. We quantify potential biases arising from temporal mismatch between ice elevation and ice velocity measurements by adjusting our thickness estimates using a glacier thinning rate of $\frac{\partial H}{\partial t} = -0.1 \text{ m d}^{-1}$ during summer months (May through September) and $\frac{\partial H}{\partial t} = 0.05 \text{ m d}^{-1}$ during non-summer months according to observations from Helheim and Kangerdlussuaq glaciers by Kerhl et al. (2017) and performing the same calving model

calibrations as executed with the observed thicknesses. Finding negligible differences in calving model calibrations and performances when input with time-corrected ice thicknesses, we only report results using original ice thickness and velocity measurements.

We convert surface strain rates derived from ice flow speeds to ice stresses using n = 3 and the temperature-dependent rate parameter, B = 324 $kPa^{-1}$ $yr^{-1/3}$, that corresponds to an ice temperature of –5 °C (Cuffey and Paterson, 2010). Though the depth-averaged ice temperature of most glaciers in Greenland is colder than –5 C, borehole observations suggest that the ice in surface and basal regions where crevasses are expected to form near glacier termini may generally be in range of –2 to -10 C (Iken et al., 1993; Luthi et al., 2002).

We calculate observed frontal ablation rates as the difference between glacier length change over time and ice velocity,

$$u_f = \frac{\partial l}{\partial t} - u_i, \tag{16}$$

where $\frac{\partial l}{\partial t}$ is the distance between two traced terminus margins from satellite images divided by the time between satellite images and $u_i$ is the ice velocity. The two satellite images for terminus traces are coincident with or fall within the dates of the two satellite images employed in the generation of the corresponding ice velocity map. Terminus margins are digitized by hand from Landsat and Sentinel satellite images using the Google Earth Engine digitization tool developed by Lea (2017). The change in time between terminus traces is typically 11-35 days, depending on the corresponding velocity observation period and the availability of suitable satellite imagery. Similar to Luckman et al. (2015), we calculate length change rate and ice velocity along a series of 20 parallel profiles oriented with ice flow and spaced 100 m apart that span the center 2000 m of the terminus width. By averaging frontal ablation rates across the middle 2000 m of the glacier, we reduce the effect of large individual calving events that only impact one part of the terminus and obtain a frontal ablation rate that represents the behavior of the glacier where it is thickest and fastest. Errors arising from digitization of satellite images are estimated to be on the order of 30m, which combined with reported ice velocity errors, results in frontal ablation rate uncertainties of less than 1.5 m $d^{-1}$.

Observed terminus positions used to evaluate calving position models are identified as the calving cliff crest as opposed to the intersection of the calving cliff and the waterline. We

frequently observe in the ATM surface elevation measurements from April/May that sample glaciers terminate in a several-hundred-meter ramp of ice blocks sloping down from the cliff top to the waterline. Since we do not expect this ice ramp to contribute to the glacier stress balance in the same manner as intact glacier ice, it is not included in our evaluation of calving position models.

Input data for the six calving models are interpolated onto 1-D center profiles that follow ATM flight paths up the glacier middle, thus capturing the behavior of the glacier where it is likely thickest and fastest. Measures of calving model accuracy are obtained through comparison between modeled and observed calving front positions or calving rates along the 1-D profiles. Our 1-D terminus position method is consistent with methods employed in studies quantifying terminus change at outlet glaciers in Greenland (e.g. Bevan et al., 2012). Observations of dynamic changes at marine-terminating glaciers show that on inter-annual time scales, terminus retreat and stabilization frequently initiate from the center (McNabb and Hock, 2014), which suggests that capturing glacier behavior along the centerline is critical for accurate representation of dynamic changes. Furthermore, terminus change studies reveal that the position of the terminus rarely varies by >1 km across its entire width (Murray et al., 2015 Catania et al., 2018): a difference that is currently below the resolution of a single grid cell for all but one Greenland Ice Sheet model (Goelzer et al., 2018). For these reasons, we feel that our 1-D profile methods are suitably representative of dynamic terminus processes for the purposes of evaluating calving criteria.

Although Operation IceBridge ATM ice elevation data cover nearly 100 glaciers, the requirements of near-coincident ice elevation and ice velocity data for glaciers with reasonably accurate bed elevation estimates significantly reduces the number of outlet glaciers in Greenland with sufficient data for our analysis. Of the roughly 200 outlet glaciers in Greenland, we identify 50 glaciers that have one set of suitable observations against which to evaluate calving models (Figure 2.1). WV DEMs with intra-annual temporal resolution are available for several of Greenland's well-studied glaciers, which allows us to assess the effects of temporal sampling on our analysis.

We evaluate each calving model against terminus variability across spatial and temporal scales using a set of spatially-distributed observations and a set of temporally-distributed observations. The spatially-distributed observation set consists of a single set of

measurements from all 50 sample glaciers. These glaciers span a range of glacier characteristics and environmental settings, exemplified by varying ice thicknesses (Howat et al., 2014), ice velocities (Joughin et al., 2010), calving styles (Vietch and Nettles, 2012; Fried et al., 2018), air temperatures (which affect both ice temperature and melt rates; Cowton et al., 2018), ocean water temperatures (Straneo et al., 2012), and recent position changes (Murray

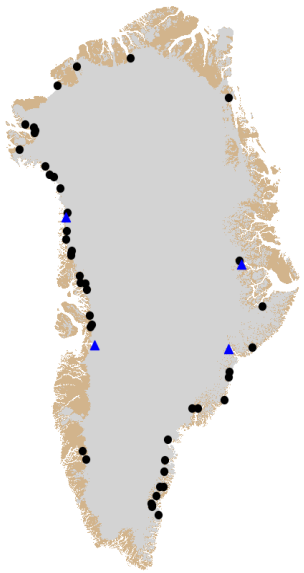

Figure 2.1: Sample glacier locations in Greenland. Black circles represent glaciers with one observation available that contribute to spatially-varying data set. Blue triangles denote glaciers that have an additional 15 repeat observations that contribute to temporally-varying data set.

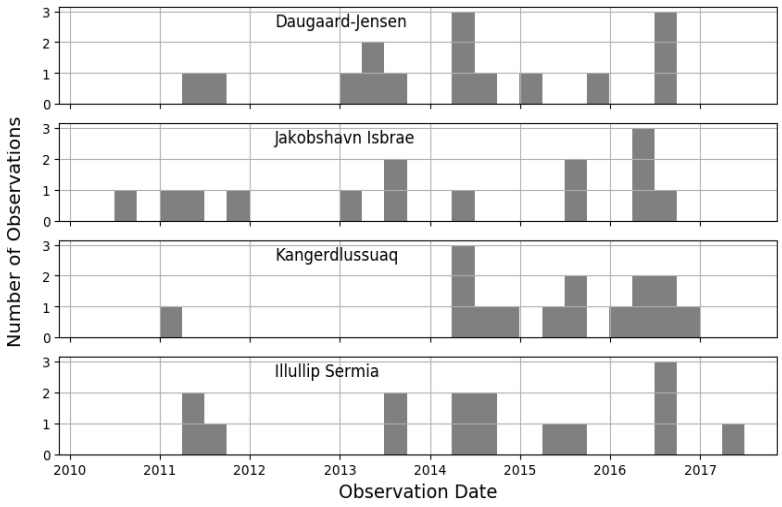


Figure 2.2: Temporal distribution of time series observations at four sample glaciers shown in blue triangles in Figure 2.1.

et al., 2015), such that our 50 sample glaciers broadly represent the marine boundary of the Greenland Ice Sheet as a whole. Most of our sample glaciers are concentrated in the NW and SE sectors of the ice sheet, which in combination account for approximately 80% of total ice sheet dynamic discharge (Enderlin et al., 2014), although we include glaciers around the entire ice sheet periphery. Observations at sample glaciers consist of bed elevation and coincident ice elevation and ice velocity observations that are from May/June and span the years 2009 to 2017.

The temporally-distributed observation set consists of 15 observations from Jakobshavn Isbrae, Kangerdlussuaq, Illullip Sermia, and Daugaard-Jensen glaciers for a total of 60 observations. Collectively, these observations span the winter, summer, and shoulder seasons during the years 2010 to 2017 as shown in Figure 2.2. Frontal ablation rates at outlet

glaciers vary from virtually a complete cessation in winter to the loss of several kilometers of ice in a single day during early summer (Amundson et al., 2010; Robel, 2017). It is therefore expected that the performance of a calving model calibrated during May/June may share little similarity with the performance of the same model during other seasons. The four glaciers selected exhibit some of the largest seasonal variability in observed frontal ablation rates and terminus position in Greenland (Bevan et al., 2012; Schild and Hamilton, 2013; Casotto et al., 2015; Moon et al., 2015; Kehrl et al., 2017) and thus provide an approximate upper bound on temporal variability across Greenland.

### 2.3 Calving Model Calibration and Evaluation

We seek to identify the best value of each model's free parameter by testing models with parameters drawn from a wide range of values that are inclusive of those recommended by the literature. We also assess model performance at broad spatial and temporal scales. We first draw on each observation of the 50 individual sample glaciers in the spatially-distributed data set to empirically calibrate each calving model. We refer to the parameter that yields the most accurate terminus position or calving rate for each observation as the *observation-optimized* parameter. For calving rate models, model accuracy is measured according to the *misfit rate*, defined as the difference between modeled and observed calving rates. The accuracy of calving position models is determined by the 1-D along-profile distance between modeled and observed terminus positions, referred to as the *misfit distance* (Figure 2.3). Although misfit rates can be positive or negative, only positive misfit distances (indicative of retreat) are possible when testing calving position models against observed glacier geometries because there are no thickness and speed observations down-fjord of termini, making it is impossible to have a modeled terminus position that is seaward of the observed terminus. This particular issue is not present when evaluating calving parameterizations in a numerical glacier model since the model advances the glacier front until advance is stopped by the calving criteria.

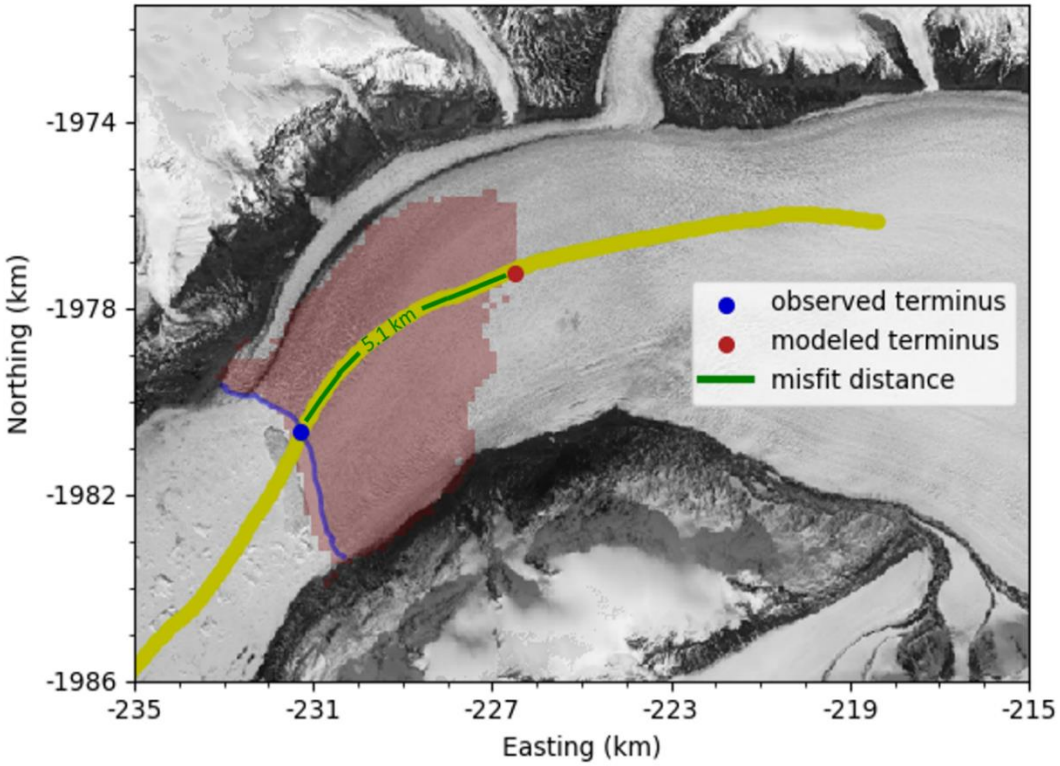


Figure 2.3: Diagram of example misfit measurement for calving position models shown under with example criteria of HAF model and critical excess ice height, $h_c$=50 m. Red shading depicts unstable glacier ice that is assumed to calve off according to the HAF criteria. Modeled and observed terminus positions are interpolated onto center profile line such that misfit distance is represented by 1-D offset between points. Note that by using only observations data for model input, calving position models can only predict terminus positions co-located or up-fjord of observed terminus point. Down-fjord positions and associated misfits are not quantifiable in this study. Background is Landsat 8 image from 03 May 2016.

Calving models are then calibrated to the entirety of the Greenland Ice Sheet by identifying *spatially-optimized* parameter values that minimize the total misfit between model predictions and observations at all 50 sample glaciers. This calibration process reflects the current need in ice sheet models for a simple, calibrated, universal boundary criterion that may be applied to the entire Greenland ice sheet. Spatially-optimized parameter values are defined as those that yield a median of individual glacier misfits nearest to 0 m for calving position models and 0 m $d^{-1}$ for calving rate models. Using spatially-optimized parameter values, each calving model configuration under-predicts the calving position or calving rate at 25 glaciers and over-predicts the calving position or calving rate at the other 25 glaciers; hence offering the best compromise in model performance across all 50 sample glaciers.

Lastly, we investigate how calibrated parameter values may vary through time at individual glaciers, and consequently, how representative the spatially-optimized model configurations are of ice sheet terminus dynamics over time. For each calving model, we identify observation-optimized parameter values for the four sample glaciers in the temporally-distributed observation set. We then determine *temporally-optimized* parameter values for each calving model and for each glacier in the temporally-distributed observation set. Temporally-optimized parameter values are defined as the value that yields a median misfit nearest to 0 m for calving position models and 0 m $d^{-1}$ for calving rate models across all 15 observations at a given sample glacier.

We assess the performance of spatially-optimized and temporally-optimized calving models in terms of model bias, model uncertainty, and model sensitivity. Model bias measures the difference between the median modeled misfit ($m_{50}$) and zero misfit. Calving models that exhibit a median model misfit of 0 m or 0 m $d^{-1}$ will therefore have no model bias. Model uncertainty measures the spread of individual glacier misfits around the median misfit value. We assess model uncertainty for calving rate models via the 25$^{th}$ and 75$^{th}$ percentiles ($m_{25}$ and $m_{75}$) of rate misfit such that model bias and uncertainty are given in the form: $\delta_{model} = m_{50} \pm^{m_{75}-m_{50}}_{m_{25}-m_{50}}$ m $d^{-1}$. If $m_{50} = 0$ m $d^{-1}$, $\delta_{model}$ reduces to $\delta_{model} = \pm^{m_{75}}_{m_{25}}$ m $d^{-1}$. For calving position models, we can determine an optimized parameter that results in a median misfit of 0 m, but our analysis is unable to quantify misfits associated with predicted termini down-fjord of the input observation domain. We therefore make the assumption that over-advanced misfit distances are comparable in magnitude to the over-retreated misfits such that $\delta_{model} = m_{50} \pm (m_{75-}m_{50})$ m $d^{-1}$. More complete quantification of over-advanced misfits requires realistic numerical extrapolation of glacier extents down-fjord; a process that involves precise knowledge of local ice flow parameters across 50 outlet glaciers and is thereby beyond the scope of this study. However, the preponderance of shallow sills followed by deeper water depths down-fjord of current glacier fronts likely constrains the potential for large dynamic advances at many outlet glaciers (Rignot et al., 2016b), and thus provides a physical basis for our assumption regarding over-advanced misfit distances. Finally, we calculate model sensitivity, which provides a measure of the change in model bias resulting from a small change in the free parameter value. In the likely occurrence

that our analysis does not represent a perfect characterization of spatially- and temporally-optimized model parameters, we seek a model that will be relatively insensitive to small perturbations in parameter value.

Our empirical approach to quantifying calving model uncertainties enables direct inter-comparison of calving model bias, uncertainty, and sensitivity at the ice sheet scale. Comparison of these three quantities reveals relative calving model accuracies and suitability for use as frontal boundary criteria in prognostic models of the Greenland Ice Sheet. However, since no direct conversion exists between calving rate error and terminus position error without integration over time, calving rate model uncertainties and sensitivities are not directly comparable to those exhibited by calving position models. To reconcile this shortcoming, we discuss expected calving model errors when calving rate models and calving position models are implemented in numerical glacier models and projected over future time scales.

## 3. Results

### 3.1 Observation-optimized calibrations

We first determine observation-optimized parameters for each of the 50 sample glaciers by identifying the free parameter value that optimizes the fit between modelled and observed calving behaviors. We find that, through varying calving model parameter values, we are able to accurately reproduce terminus conditions (i.e., with zero misfit) at almost all glaciers with five out of six calving models tested here (Figures 3.1 and 3.2). We furthermore find that calving model accuracy at individual glaciers is highly dependent on parameter value.

#### 3.1a: Calving position models

The HAF, FAF, and CD models all reproduce most sample glacier terminus positions with high accuracy when using model parameter tuned to each individual glacier. We find that 11 of the 50 sample glaciers feature short, ungrounded, terminal extensions in the ATM ice elevation measurements from April/May. The other 39 glaciers are grounded between 1 m and 80 m above flotation, or similarly between a water depth fraction of 0.01 and 0.4 (Figure 3.1a and 3.1b). Perfect simulation of terminus position by the HAF and FAF models is therefore achieved at 39 of the 50 sample glaciers using observationally-optimized parameter values, though we note that for 7 of the 11 floating termini the modeled termini positions are less than 1 km from the observed positions. The HAF and FAF models perform particularly poorly when applied to Kangerlussuaq and Petermann glaciers, which feature floating ice tongues of approximately 5 km and 60 km in length, respectively. Observationally-optimized $h_c$ (critical height above buoyancy) and $f$ (fraction above flotation) parameter values at glaciers in northern Greenland are generally smaller than values for glaciers in southern Greenland, a pattern that is broadly consistent with the occurrence of floating ice tongues at northern outlet glaciers.

The CD model exactly reproduces terminus position at 48 of 50 sample glaciers, irrespective of flotation state. Water depth ($d_w$) values required to reproduce observed terminus positions range from 0 m up to 100 m across the 50 sample glaciers (Figure 3.1c). In the case of Kangerlussuaq and Petermann glaciers, the CD model can reproduce observed terminus positions if it is assumed that surface crevasses are filled with 26 m of water at

Kangerlussuaq and 43 m at Petermann glacier. No obvious spatial pattern exists in the distribution of observationally-optimized $d_w$ values at the 50 sample glaciers, though the largest $d_w$ values are associated with glaciers located in southern Greenland (Figure 3.1c).

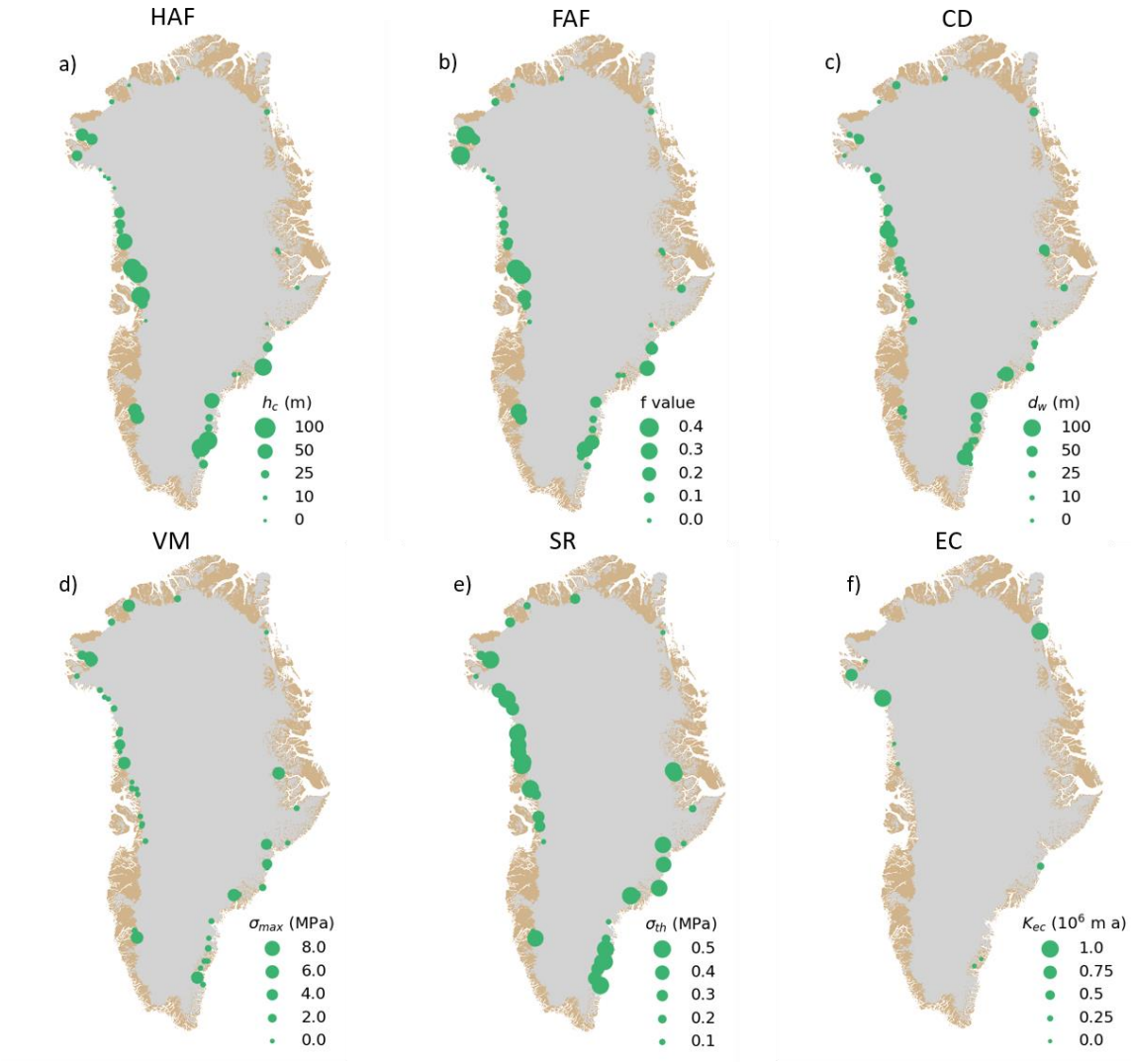


Figure 3.1: Observation-optimized parameter values for six calving models in (a) – (f) . Note variability in glacier-specific optimal parameters. Eigencalving model in (f) is only valid at nine glaciers around Greenland due to the model requirement of that strain rate eigenvalues must be positive to incite calving.

### 3.1b: Calving rate models

As with the calving position models, we compare modeled calving rates to observed frontal ablation rates from May/June at all sample glaciers to determine how well calving rate models can simulate frontal ablation rates in Greenland. Observed frontal ablation rates vary

from 0 m $d^{-1}$ to 69 m $d^{-1}$, suggesting that these observations are from a time when frontal ablation at glacier fronts is highly variable across the ice sheet. While frontal ablation is low at some glaciers, such as Petermann glacier, vigorous ablation has commenced at other glaciers, as at Zachariae Isstrom. Accounting for the observed variability in frontal ablation rates across Greenland provides a particularly challenging test for the three calving rate models investigated in this study.

We find that the VM model accurately predicts frontal ablation rates from all 50 sample glaciers that range from 0 m $d^{-1}$ to 69 m $d^{-1}$. However, at 8 sample glaciers, accurate simulation of frontal ablation rates by the VM model is only achieved using extremely high (> 5 MPa) values for $\sigma_{max}$. If $\sigma_{max}$ represents ice tensile strength as in Morlighem et al. (2016), values of $\sigma_{max}$ greater than 3 MPa are likely unrealistic in Greenland (Petrovic, 2003). The VM model struggles in cases where observed ice velocities are on the order of tens of m $d^{-1}$ but observed frontal ablation rates are near 0 m $d^{-1}$, since such a condition requires that $\sigma_{max}$ greatly exceed the tensile von Mises stress at the terminus, $\sigma_{vm}$. The SR model accurately reproduces frontal ablation rates at 38 of 50 sample glaciers, but over-estimates frontal ablation rates at 5 glaciers and under-estimates the frontal ablation rates at the remaining 7 glaciers. For these 12 glaciers there is no value of the ice strength threshold parameter $\sigma_{th}$ that yields zero misfit.

The SR model is markedly less sensitive to choice of free parameter value than the VM model, which may contribute to its inability to reproduce exact frontal ablation rates at 12 of 50 glaciers. Variation of model parameters other than that which we explored here (see Mercenier et al., 2017) has the potential to further improve the model fit. Modeled calving rates in the SR model for individual glaciers exhibit a smaller range than for the VM model since the maximum modeled calving rate for a particular glacier from the SR model is a pre-determined function of the H/D ratio of a particular glacier, and thus cannot be enhanced by any value of $\sigma_{th}$. The spatial distributions of optimal $\sigma_{max}$ and $\sigma_{th}$ values at sample glaciers do not reveal any obvious spatial pattern, but suggests that most observationally-optimized $\sigma_{th}$ values lie within a narrower range than optimal $\sigma_{max}$ values (Figures 3.1d and 3.1e).

The EC model exactly reproduces observed frontal ablation rates at 9 of 50 sample glaciers using free parameter values of that vary by several orders of magnitude between 0.02 to $10^6$ m a (Figure 3.1f). Due to the requirement that there must be tensile stretching in both

principle directions at the glacier terminus to induce calving, the EC model is invalid at 41 of 50 sample glaciers. This is not a surprising finding given that most Greenland outlet glaciers are confined to narrow fjords that suppress transverse ice flow (Morlighem et al., 2016). For the 9 glaciers where the EC model is valid, the sensitivity of modeled calving rates to the choice of parameter *K* enables the EC model to account for highly variable frontal ablation rates. However, the observationally-optimized values for *K* span a wide range, precluding the existence of a single *K* value that produces accurate simulation at all 9 glaciers (Figure 3.1f). Given the limited applicability of the EC model to Greenland outlet glaciers, we do not include the model in all subsequent results.

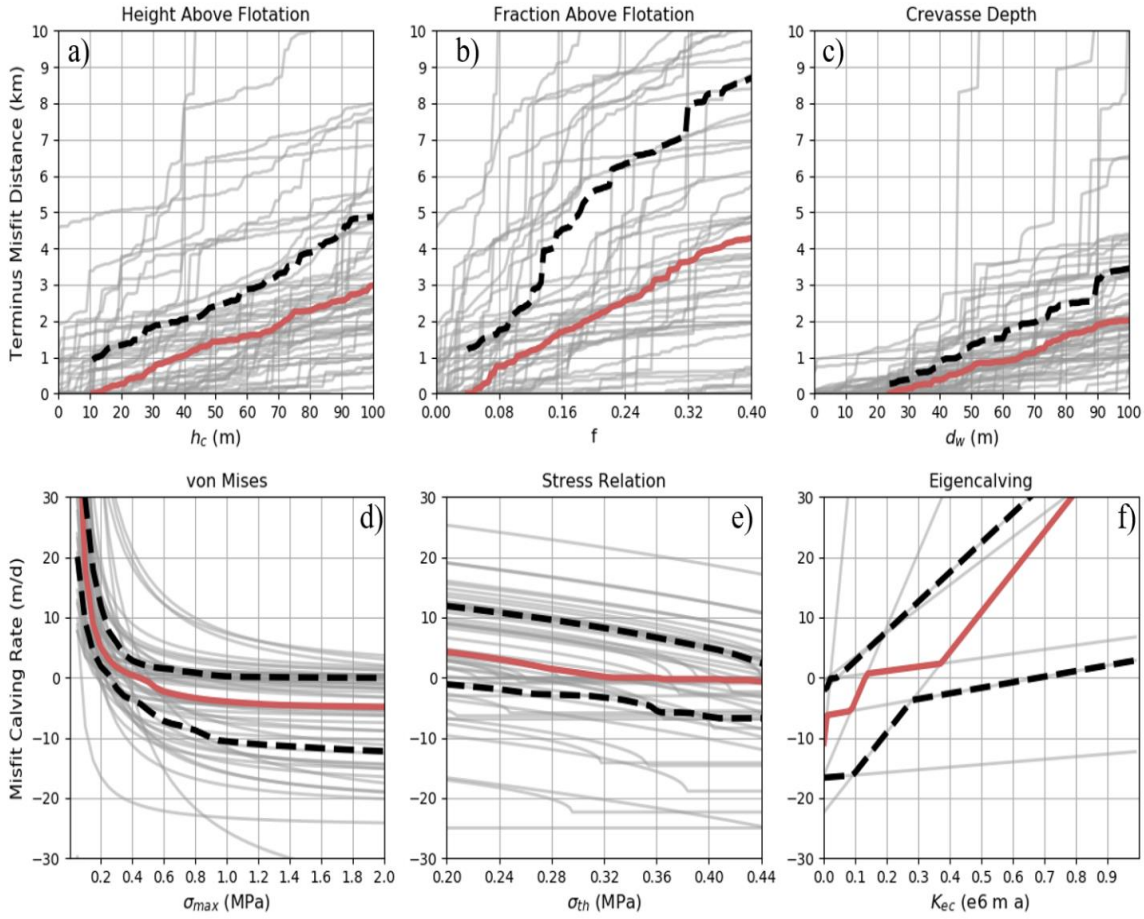


Figure 3.2: Calving position models in (a) – (c) and calving rate models in (d) – (f) showing calibration of free parameters to 50 sample glaciers. Red line tracks the median misfit, black lines bracket model uncertainty, defined as interquartile range in (d) – (f) and 75$^{th}$ percentile in (a)– (c). Light gray lines depict calibration curves for each individual glacier. Ice-sheet wide optimal parameters for each model are identified as parameter which yields a median misfit of 0 for all sample glaciers.

### 3.2. Spatially-optimized calibrations

The empirical calibration of each model to the collective set of 50 sample glaciers reveals the single optimal parameter value within each model that minimizes the overall misfit at the ice sheet scale. With the exception of the EC model, we find that all calving models investigated in this study can be successfully calibrated to produce a median misfit of 0 for all 50 sample glaciers using a fixed, spatially-optimized parameter value (figure 3.2). The CD model exhibits the lowest model uncertainty amongst the tested position models while the VM model features the lowest model uncertainty amongst the calving rate models. Parameter values and associated model misfits are given in Table 3.1.

| Model | HAF | FAF | CD | VM | SR |
|---|---|---|---|---|---|
| **Spatially-optimized parameter** | $h_c = 11$ m [7 to 19] | $f = 0.04$ [0.01 to 0.08] | $d_w = 24$ m [22 to 24] | $\sigma_{max} = 0.45$ MPa [0.36 to 0.52] | $\sigma_{th} = 0.33$ MPa [0.28 to 0.46] |
| **Model Uncertainty** | ± 0.9 km [0.9 to 1.2] | ± 1.3 km [1.2 to 1.3] | ± 0.3 km [0.3] | $\pm^{2.4}_{4.2}$ m d$^{-1}$ [$\pm^{2.4}_{3.8}$ to $\pm^{3.8}_{5.2}$] | $\pm^{8.0}_{3.5}$ m d$^{-1}$ [$\pm^{2.4}_{3.9}$ to $\pm^{8.0}_{6.6}$] |

Table 3.1: Performance of spatially-optimized calving models to 50 sample glaciers. Bracketed parameter values and model uncertainty show the ranges that exist when errors in bed elevation and temporal mismatch between ice elevation and velocity measurements are taken into account.

#### 3.2a: Calving position models

Using observations from our 50 sample glaciers, we find that the three calving position models all perform well at the ice sheet scale. The CD model with $d_w = 24\ m$ estimates the terminus position at 50% of the sample glaciers to within 0.3 km and 90% to within 1 km (Figure 3.3c). Only two glaciers, Issuussarsuit Sermia and Humboldt Gletcher, in the NW of Greenland exhibit modeled terminus positions more than 1 km away from the observed terminus positions when $d_w = 24\ m$ (1.3 km and 1.2 km respectively). We note from Figure 3.2c that the spatially-optimized CD model has low model sensitivity: with an approximate doubling of crevasse water depths to $d_w = 50\ m$, the CD model still simulates terminus positions at 50% of sample glaciers to within 1 km. The HAF model with $h_c = 11\ m$ estimates terminus position at 50% of the sample glaciers to within 0.9 km which is

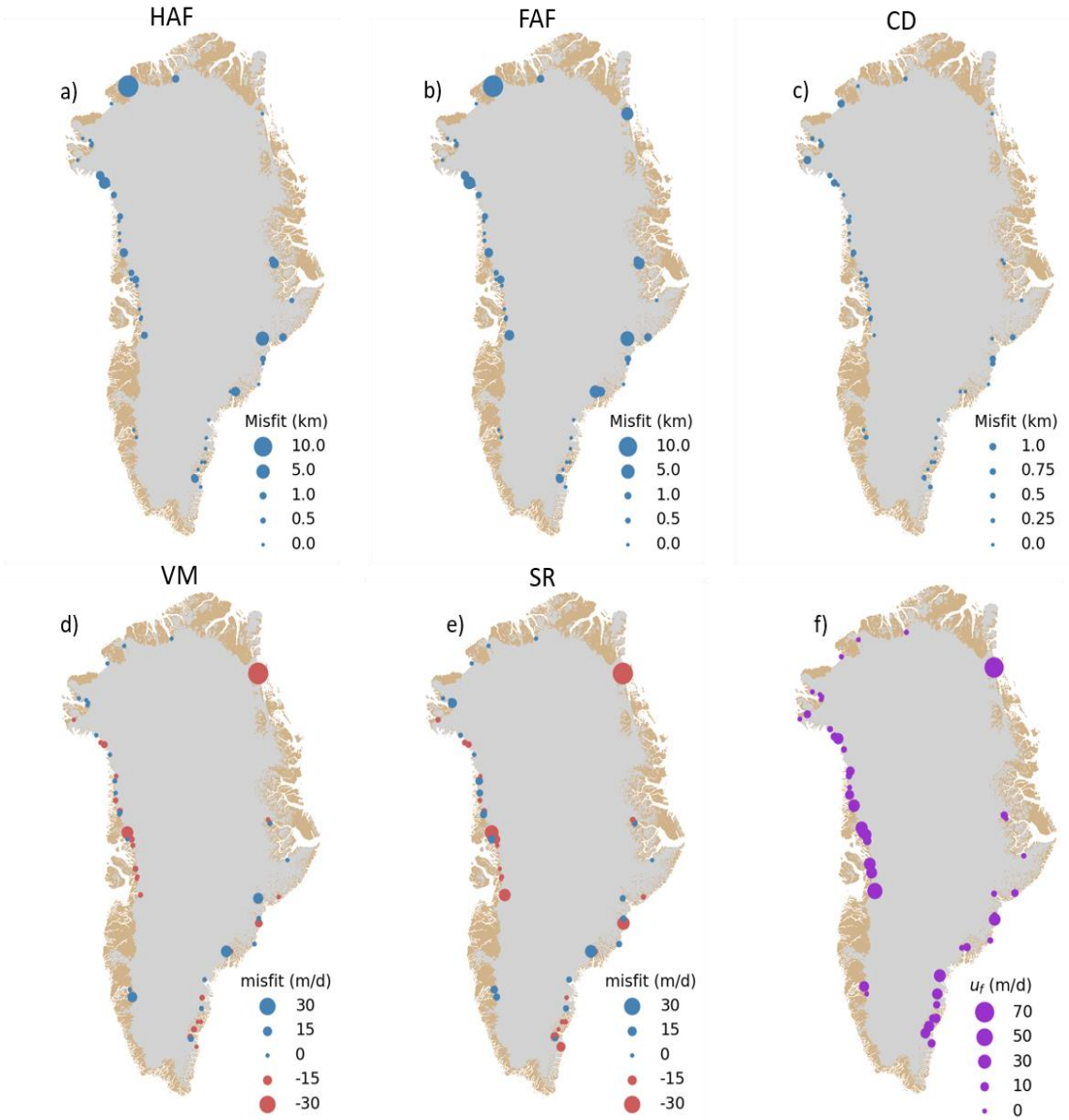


Figure 3.3: Model misfits at individual glaciers using spatially-optimized model configurations. Calving position models in (a) – (c) and calving rate models in (d) and (e). Panel (f) shows observed frontal ablation rates during May/June. Note that symbol size scales in (a) – (c) are equivalent. The exceptionally large (69 m/d) observed frontal ablation rate in Northeast of Greenland belongs to Zachariae Isstrom glacier.

slightly better than the FAF model with $f = 0.04$ (1.2 km at 50% of sample glaciers). Expectedly, the HAF and FAF models exhibit identical deficiencies at glaciers featuring floating termini, such as Kangerdlussuaq and Petermann glaciers (Figure 3.3a and 3.3b). The HAF model notably outperforms the FAF model at several of Greenland's largest glaciers, including Jakobshavn Isbrae, Helheim Glacier, and Zachariae Isstrom. These glaciers are all relatively thick and close to buoyancy, such that the ice thickness fractions above buoyancy

(f) are relatively small near the glacier termini while the heights above buoyancy ($h_c$) are comparably large. Expectedly, the CD model outperforms the HAF and FAF models at glaciers with floating termini, but the CD model also proves to be more accurate than the flotation models at almost all grounded sample glaciers as well, with the exception of several glaciers in the Northwest of Greenland.

### 3.2b: Calving rate models

The VM calving model with a tensile stress threshold, $\sigma_{max} = 0.45$ MPa reproduces observed frontal ablation rates at 50% of sample glaciers to within an uncertainty of $\pm^{2.4}_{4.2}$ m d$^{-1}$ and at 90% of sample glaciers to within $\pm^{12.8}_{11.1}$ m d$^{-1}$ (table 3). The ice-sheet wide accuracy of the VM model is similar for $\sigma_{max}$ values between 0.4 and 0.5 MPa, though model bias and uncertainty both increase considerably outside of this range (Figure 3.3d). The SR model with a spatially-optimized $\sigma_{th}$ value of $\sigma_{th} = 0.33$ MPa reproduces 50% of observed frontal ablation rates to within uncertainty of $\pm^{8.0}_{3.5}$ m d$^{-1}$ and reproduces 90% of observed rates to within $\pm^{13.7}_{21.5}$ m d$^{-1}$. SR model bias is notably not very sensitive to increases in the value of $\sigma_{th}$, likely owing to fact that modeled calving rates become 0 m d$^{-1}$ when $\sigma_{th}$ exceeds the principle ice stress $\sigma_1$. The spatially-optimized VM and SR models under-estimate frontal ablation rates at Zachariae Isstrom by more than 50 m d$^{-1}$ and at Ingia Isbrae by more than 20 m d$^{-1}$, while simultaneously over-estimating frontal ablation rates at Helheim glacier by more than 20 m d$^{-1}$. We also observe that both models under-estimate calving rates at glaciers in central west Greenland where observed frontal ablation rates are relatively high (15 to 30 m d$^{-1}$), but accurately estimate calving rates at glaciers in the North/Northwest of Greenland where observed frontal ablation rates are less than 10 m d$^{-1}$ (Figures 3.3d and 3.3e). These model performance patterns are in contrast with the absence of spatial patterns exhibited by the spatially-optimized calving position models (Figures 3.3a – 3.3c)

### 3.3 Observation-optimized calibrations to temporally-varying data

The positions of outlet glacier termini in Greenland typically fluctuate by < 1 km per year (Moon et al., 2015; Bartholomaus et al., 2016; Catania et al., 2018) but can change by up to several kilometers on an annual basis at the largest glaciers, such as Jakobshavn Isbrae,

(Cassotto et al., 2015). We observe that short-term (sub-monthly to monthly) frontal ablation rates vary from 0 m $d^{-1}$ to roughly 50 m $d^{-1}$ over seasonal time scales, though at Jakobshavn Isbrae and Kangerdlussuaq glaciers we observe several short-term frontal ablation rates in excess of 100 m $d^{-1}$. Although large, inter-annual changes in terminus position are possible and have been recently observed at Greenland outlet glaciers (e.g. Murray et al., 2015) the four glaciers in our temporally-distributed data set do not exhibit any sustained inter-annual dynamic changes, with the exception of a slight (< 3 km) advance at Jakobshavn Isbrae over the period 2011 to 2017 (Khazendar et al., 2019). Similarly, we do not observe evidence of inter-annual variability in observed frontal ablation rates at the four glaciers in the temporally-distributed data set, though we note that such variability is widespread in recent observations of Greenland (Moon et al., 2012; Howat and Eddy, 2012; Csatho et al., 2014).

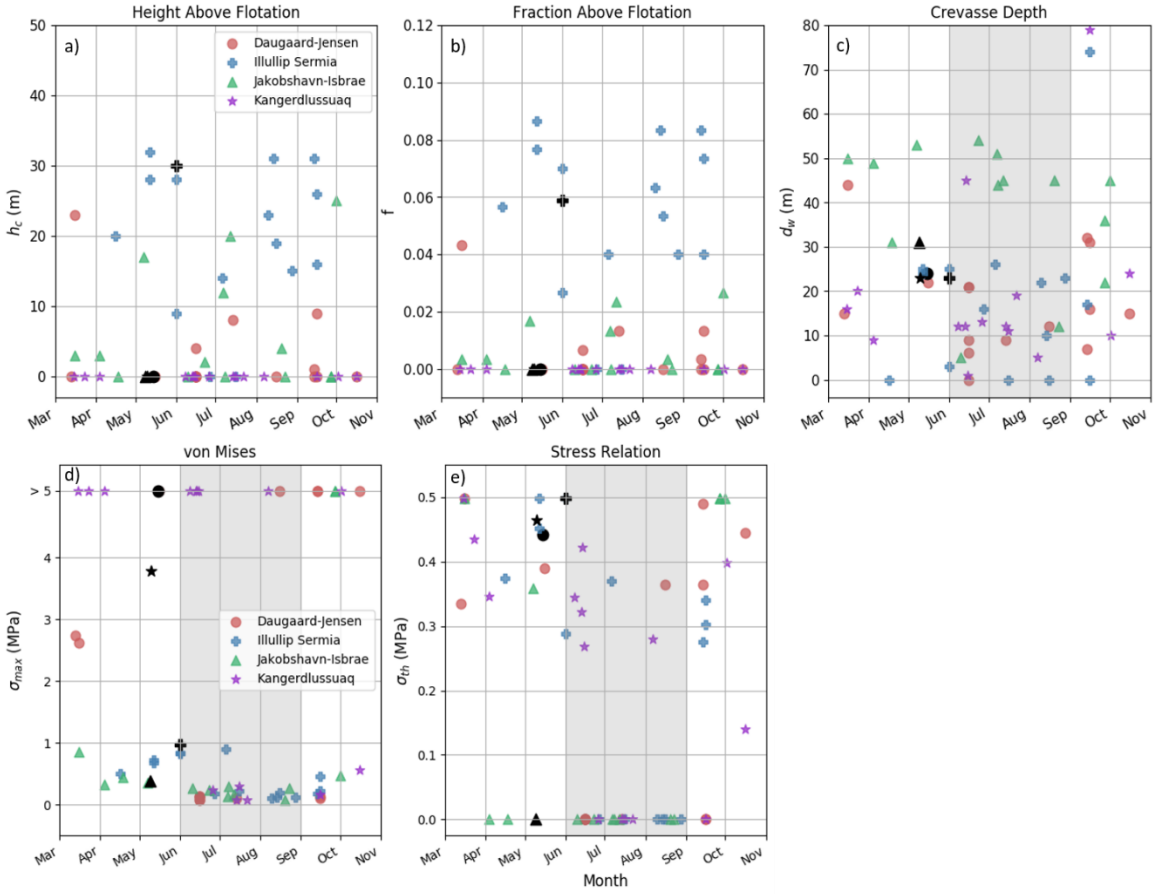


Figure 3.4: Temporal variability in individual glacier optimal model parameters. Colored symbols represents observationally-optimized parameter value calibrated against glacier observations that vary in season. Peak glacial runoff period from June through September is shaded gray for models that incorporate ice stresses. Filled black symbols depict observationally-optimized parameter values calibrated to spatial data set and are shown for comparison.

Optimal model parameter values change to meet the seasonal and inter-annual changes in terminus position and frontal ablation rates in our observation data, as shown in Figure 3.4. The spatially-optimized model parameters we identify using measurements during May/June therefore may not be the most accurate parameter values to use during a different time of year or during a different year altogether. Indeed, we find that the temporal variability in observation-optimized model parameters at four individual glaciers is considerable, and similar in magnitude to the observation-optimized parameter variability observed across the entire ice sheet.

**3.3a Position models: temporal variability**

Observationally-optimized values for $h_c$ and f exhibit similar variability over time for Jakobshavn Isbrae, Illullip Sermia, Daugaard-Jensen, and Kangerdlussuaq glaciers. Independent of season, observation-optimized $h_c$ and f values vary by roughly 20 m and by a fraction of 0.02 at all glaciers except Kangerdlussuaq, which features a floating ice tongue for the duration of the observation period and therefore has consistent optimized values of $h_c = f = 0$. Comparatively, the CD model exhibits greater variability in observational-optimized parameter values, with optimized $d_w$ values fluctuating by more than 40 m at all four glaciers. Importantly, we find that optimized $d_w$ values vary independently of season, a result that is in conflict with the physical meaning of $d_w$ as the crevasse water depth, which is expected to vary seasonally as runoff is routed to surface crevasses. Observationally-optimized parameters from the spatial validation data set are shown in black symbols in Figure 3.4. For the three position models, these calibrated parameters are within the range exhibited by observationally-optimized parameters from the temporal validation data set. This indicates that for position calving models, spatially-optimized parameter values that are empirically calibrated to observations from May/June are likely to be broadly representative of calving conditions on annual time scales.

**3.3b: Rate models: temporal variability**

Observation-optimized parameter values calibrated to temporally-distributed observations for the VM model span the full range (0 MPa to > 5 MPa) of tested parameter values at three of the four sample glaciers in the temporal data set (Figure 3.3d). That is, the

observation-optimized values of $\sigma_{max}$ over 15 observation dates at a single glacier are equal in spread to that exhibited by observation-optimized $\sigma_{max}$ values across 50 sample glaciers in the spatially-distributed data set. Despite this temporal variability, there is a discernible seasonal influence on observationally-optimized parameters at Jakobshavn Isbrae and Illullup Sermia glaciers. The smallest $\sigma_{max}$ values at Jakobshavn Isbrae are found during estimated peak runoff months, which are coincident with peak observed frontal ablation rates. Similarly, the minimum optimal $\sigma_{max}$ values for Illullip Sermia glacier are all found during August, coincident with the largest observed frontal ablation rates at Illullip Sermia. Observationally-optimized $\sigma_{max}$ values at Kangerdlussuaq glacier exhibit a dichotomy between extremely large ($\sigma_{max}$ > 5 MPa) and small ($\sigma_{max}$ < 1 MPa) values, irrespective of observation month. Correspondingly, we find that observed frontal ablation rates at Kangerdlussuaq glacier are almost all either exceptionally large rates ($u_f$> 50 m $d^{-1}$) or negligible small ($u_f$ < 2 m $d^{-1}$), suggesting the occurrence of km-scale calving events punctuated by periods of quiescence.

Observational-optimized $\sigma_{th}$ values in the SR model span the full tested parameter range (0 to 0.5 MPa) for all four glaciers in the temporal validation data set (Figure 3.4e). As is the case with $\sigma_{max}$ parameter in the VM model, the temporal variability in observational-optimized $\sigma_{th}$ values in the SR model at any of the four temporal set glaciers is equal to the spatial variability in observationally-optimized $\sigma_{th}$ values across all 50 glaciers. We likewise see evidence of a weak seasonal trend in optimal $\sigma_{th}$ values at Jakobshavn Isbrae, where the largest calibrated $\sigma_{th}$ values are found during minimal runoff months, and the majority of minimum $\sigma_{th}$ values are found during the peak runoff months. Likewise, minimum $\sigma_{th}$ values for Illullip Sermia are all found during August. Interestingly, there is only one observationally-optimized $\sigma_{th}$ value within the range of 0.05 MPa to 0.25 MPa for any of the four glaciers. No obvious seasonal trend is visible in optimized parameters for either the VM or SR models at Daugaard-Jensen glacier.

### 3.4 Calving model sensitivities across spatial and temporal scales

Since we find that observation-optimized parameter values in each calving model are highly variable across both spatial and temporal scales, it is necessary to consider the performance of a calving model not only in terms of its absolute uncertainty, but also in terms

of model sensitivity to changes in free parameter value. Using the criteria of model uncertainty and model sensitivity, we inter-compare the performances of calving position models and calving rates models across ice sheet spatial scales and seasonal temporal scales (Figure 3.5).

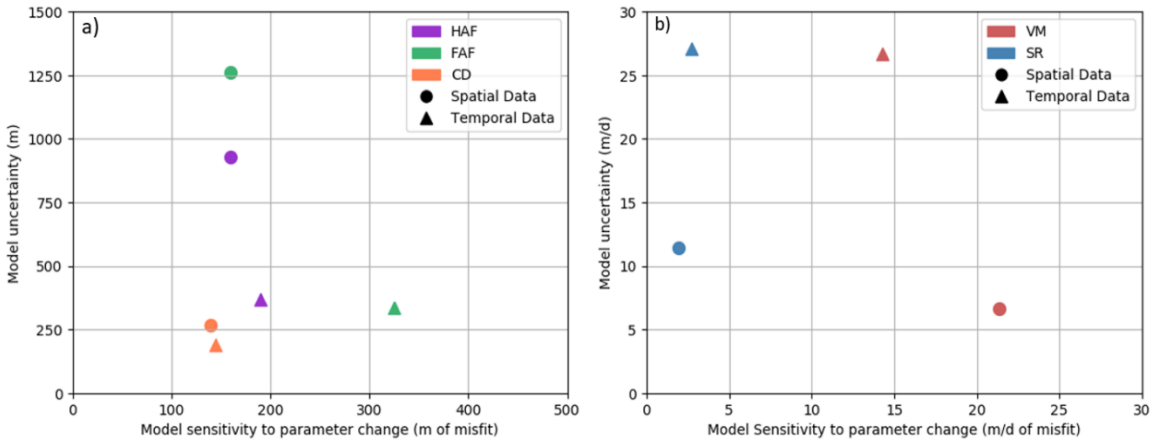


Figure 3.5: Comparison of calving model calibration sensitivity across spatial and temporal scales. Position models shown in (a) and rate models shown in (b) with temporal calibrations shown as triangles and spatial calibrations shown as circles. Y-axis measures model uncertainty in terms of 75$^{th}$ percentile in (a) or interquartile spread in (b) associated with spatially-optimized model configurations. Uncertainties associated with temporally-optimized model configurations are represented by the median uncertainty value of Illullip Sermia, Jakobshavn Isbrae, Kangerdlussuaq, and Daugaard-Jensen glaciers collectively. Model sensitivity to change in calibration parameter is depicted on x-axis according to the change in median misfit per unit parameter change. Units of parameter change defined as 25% of interquartile range of all observation-optimized parameter values included in our analysis (110 total values).

The CD calving model outperforms the HAF and FAF models across both spatial and temporal scales (Figure 3.5). When employing spatially-optimized and temporally-optimized $d_w$ values, the CD model uncertainties in terminus misfit distance are ± 270 m and ± 190 m, respectively. A change in the value of $d_w$ by 25% of the plausible range (where the plausible range is defined as the interquartile range of all observationally-optimized $d_w$ values) results in a change to the CD model bias of around 140 m for both spatially-optimized and temporally-optimized model configurations. Comparatively, the HAF model has uncertainties in terminus misfit distance of 930 m and 370 m for spatially-optimized and temporally-optimized $h_c$ values, respectively. This mirrors the finding that a much larger range of observationally-optimized $h_c$ values are needed to accurately model terminus position at 50 different outlet glaciers as compared to the range of $h_c$ values that is needed to accurately model terminus positions of an individual glacier over 15 time intervals. That is, there is more

variety in the flotation states among different glaciers than there is at a single glacier over time. The median misfits for spatially-optimized and temporally-optimized HAF model configurations are moderately sensitive to changes in the value of $h_c$. For change in $h_c$ value equal to 25% of the parameter interquartile range, model bias for the temporally-optimized HAF model changes by 190 m, while for the spatially-optimized HAF model, the model bias changes by 160 m. Interestingly, the FAF model performs comparatively worse than the HAF

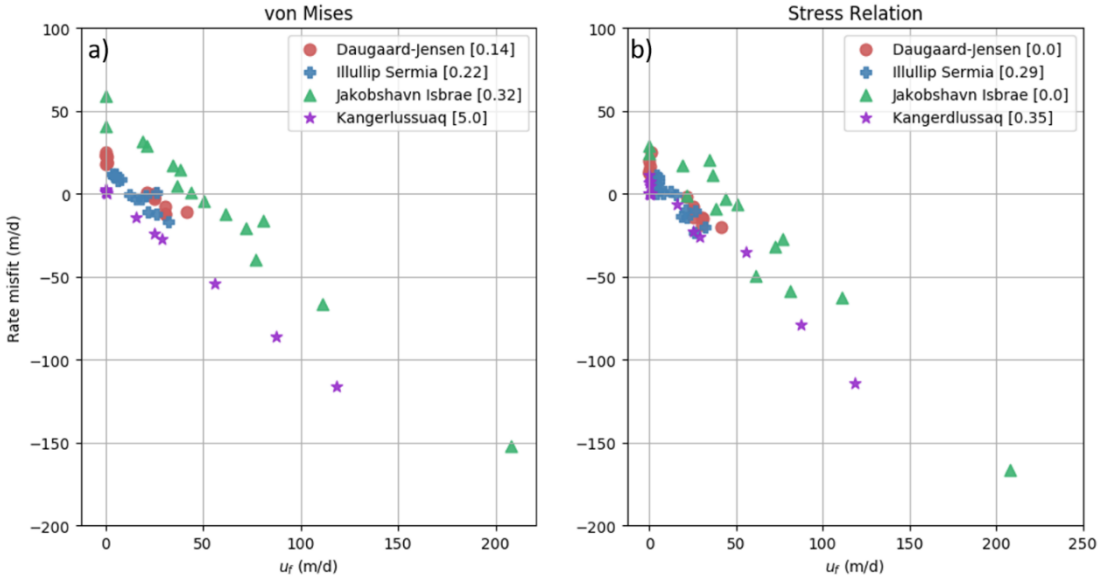


Figure 3.6: Temporally-optimized calving rate model performances against observed short-term frontal ablation rates from temporal data set. Temporally-optimized parameter values in MPa are bracketed in legend for each glacier. Neither Von Mises (a) nor Stress Relation (b) models can accurately reproduce both low ($u_f < \sim 25\ m/d$) and high ($u_f > \sim 50\ m/d$) frontal ablation rates observed over sub-monthly time scales with a single

model across spatial and temporal scales, despite similar governing principles. The temporally-optimized FAF model demonstrates comparable uncertainty to the HAF and CD models, but exhibits substantially larger model sensitivity to changes in f value. Overall, we find that the position calving models perform equally well across seasonal time scales as they do across ice sheet spatial scales.

Figure 3.5 illustrates several important features of the VM and SR calving rate models. Although the VM and SR models feature similar model uncertainties across spatial and temporal scales, the VM model has a significantly higher model sensitivity to changes in free parameter value. Specifically, a change in the value of $\sigma_{max}$, equal to 25% of the inter-quartile range of all observational-optimized $\sigma_{max}$ values, corresponds to changes of 14 m $d^{-1}$ and 22 m $d^{-1}$ in median rate misfit for temporally-optimized and spatially-optimized VM

model configurations, respectively. For a comparable modification in the value of $\sigma_{th}$, both the temporally-optimized and spatially-optimized SR model configurations exhibit model sensitivities of approximately 3 m $d^{-1}$. Importantly, the spread in model uncertainties for both temporally-optimized VM and SR model configurations are more than double the uncertainty spreads associated with spatially-optimized model configurations. This demonstrates that although the VM and SR models can be empirically calibrated to accurately reproduce observed frontal ablation rates at the ice sheet scale for a single time period, both models carry large uncertainty when reproducing short-term frontal ablation rates at individual glaciers over seasonal timescales (Figures 3.6a and 3.6b). The uncertainties in the spatially-optimized VM and SR model configurations calibrated to May/June observations are likely less than the true uncertainties associated with modeled frontal ablation rates during other times of year.

## 4. Discussion

### 4.1. Calving Model Performances

The HAF and FAF calving models are able to reproduce observed terminus positions to within roughly 1 km for most outlet glaciers tested in this study. This level of accuracy is adequate for the vast majority of ice sheet models, since at present only one ice sheet model used in centennial projections runs at a grid resolution of less than 1 km (Goelzer et al., 2018). The HAF and FAF models are unable to reproduce floating ice tongues, such as Petermann glacier in Northern Greenland, or Kangerdlussuaq glacier in the east of Greenland. For glaciers that terminate in seasonally ungrounded ice, we find that the HAF and FAF models are generally not in error by more than 1-2 km, which may be considered a negligible error when compared with ice sheet model grid resolution. Since the buoyancy heights and buoyancy fractions of individual glaciers investigated here do not change substantially over inter-annual and seasonal time scales, the uncertainties of temporally-optimized HAF and FAF model configurations are comparable to spatially-optimized model uncertainties. Accordingly, the accuracy of a spatially-optimized calibration for the HAF or FAF models will likely be stable over time, which is an important consideration for prognostic ice sheet models run over centennial time scales with a single, fixed calving criteria. As noted by others (e.g. van der Veen, 1996; Benn et al., 2007b) flotation models fail to account for situations where a glacier terminating in a stable floating ice tongue is transformed into a grounded glacier through disintegration of the ice tongue (e.g. Holland et al., 2008). Since we do not observe this phenomenon in our temporal data set, we cannot quantify the contribution of these relatively rare events to the performance of the HAF and FAF models, though we acknowledge that this phenomenon may be important for future simulations of the Greenland Ice Sheet. Overall, we find that the HAF model slightly outperforms the FAF model against the 50 outlet glaciers selected in this study. We observe that many of the thickest sample glaciers are near flotation while many of the smaller, thinner glaciers are grounded with a greater proportional of ice in excess of flotation. The five thickest sample glaciers are all optimized with $h_c$ values of 12 m or less. Accordingly, a spatially-optimized $h_c$ value more accurately accounts for the varying flotation states of sample glaciers than a spatially-optimized f value. We therefore recommend ice sheet models employing flotation criteria to employ the HAF formula using $h_c = 11\ m$.

Of the three position models tested in this study, the CD model reproduces observed terminus positions with the highest degree of accuracy. We find that the CD model is spatially-optimized to 50 sample glaciers with $d_w = 24\ m$ and has an associated model uncertainty of ± 270 m. Previous calibrations of the $d_w$ parameter achieved using observations from a single glacier or a numerical ice flow model report optimal $d_w$ values in the range of 0 m to 61 m (Otero et al., 2010; Cook et al., 2012; Otero et al., 2017; Choi et al., 2018). Although our observational-optimized $d_w$ values are in the range of reported values, there is no precedent in the literature for the approach we take to derive a spatially-optimized value of $d_w = 24$ m. We find that spatially-optimized CD model exhibits the lowest model sensitivity out of all three spatially-optimized position models, though we find cases on an individual glacier basis where an increase in $d_w$ by one meter results in substantial terminus position change similar to previous studies (Cook et al., 2012; Otero et al., 2017). We confirm previous findings that the CD model can account for ungrounded terminal ice extensions and permanent floating ice tongues (Benn et al., 2007b; Todd and Christoffersen, 2014), which is a notable advantage of the CD model over flotation criteria.

While we assume that the CD model must capture key fundamental principles of frontal ablation to demonstrate such high fidelity to observed terminus behaviors, we acknowledge the existence of two inconsistencies between the model representation and glacier observations. Firstly, our results indicate a lack of correspondence between optimal $d_w$ values and observed or expected surface crevasse water depths in near terminal regions. We expect water depths in surface crevasse to increase via water input from adjacent ice melt and runoff routing during summer months in Greenland, but there is no apparent correlation between calibrated $d_w$ value and time of year in our results. We therefore advise against the coupling of the CD model $d_w$ parameter to melt or runoff models since we find no evidence that optimal $d_w$ values follow a corresponding seasonal trend. Additionally, we find instances where optimal $d_w$ values are on the order of tens of meters, but little to no water is observed in surface crevasses near the glacier terminus using 15-m-pixel Landsat 8 satellite images. The lack of correspondence between empirically calibrated $d_w$ values and observed crevasse water depths suggests that the $d_w$ parameter acts as a heuristic stress parameter as opposed to

a realistic physical quantity. Returning to the CD model formulation, Eqs. (5) and (7) imply that ice overburden pressure at the terminus must exceed horizontal resistive stresses:

$$\rho_i g h > R_{xx}. \quad (17)$$

Although the downward pressure of water in crevasses, $P_w$, represents one additional stress that may be involved on the right hand side of Eq. (17), our results indicate that stresses other than $P_w$ likely have a greater influence on calving processes at some glaciers. As discussed by Todd and Christoffersen (2014), using a single value at all glaciers and ice depths for the rate parameter A ignores temperature-dependent variations in ice viscosity, and therefore likely generates errors in the value of $R_{xx}$. A second consideration is the reduction in the bulk density of ice caused by the presence of a crevasse field, which may lead to overestimation of the ice overburden pressure (Todd and Christoffersen, 2014). Since it is likely that the parameter $P_w$ in our analysis already accounts for stress perturbations beyond just those resulting from water pressure, we propose that a more general empirical stress parameter be implemented in Eq. (17) instead of $P_w$.

Secondly, we acknowledge inconsistencies between the Nye formulation for predicting crevasse depths and observations of true crevasse depths. The Nye formulation relies upon the assumption that surface crevasse depths are in equilibrium with surface ice stresses, though observations reported in Mottram and Benn (2009) and Colgan et al. (2016) show that observed crevasses frequently occur in regions of locally compressive stress. Even where ice stresses are extensional, crevasse depths predicted by the Nye formula (Eq. 3) are not correlated with observed depths and are often over-estimated by a factor of at least 2 on marine-terminating outlet glaciers (Enderlin and Bartholomaus, in review). These inconsistencies suggest that the CD model does not necessarily represent true surface crevasse depths. To explain the demonstrated effectiveness of the CD model in our results we consider the possibility that over-estimated crevasse depth are balanced by errors associated with over-estimation of ice overburden pressure or under-estimation of horizontal resistive stresses that arise for the same reasons just described. Alternatively, it may not be necessary for surface crevasses to penetrate fully to the waterline or to intersect with basal crevasses to induce calving, as proposed by Bassis and Walker (2012). If this hypothesis is true, over-estimated crevasse depths via the Nye formulation may balance out the error resulting from the overly-

conservative requirements that $d_s = h$ or $(d_s + d_b) = H$ for calving to occur in the CD model (Eq. 7).

The VM and SR calving rate models both reproduce spatially diverse frontal ablation rates from May/June reasonably well. For the VM model, we find a spatially-optimized value of $\sigma_{max} = 0.45\ MPa$, which is lower than the average of values reported by Choi et al. (2018) that range from 0 to 3 MPa for nine glaciers in the center West and center East of Greenland. The SR model parameter $\sigma_{th}$ is spatially-optimized to 50 sample glaciers with a value of $\sigma_{th} = 0.33\ MPa$, which is approximately double the value of $\sigma_{th} = 0.17\ MPa$ identified via calibration to a diverse set of 13 Arctic marine-terminating glaciers by Mercenier et al. (2017). Observed frontal ablation rates across the 50 sample glaciers vary by a factor of 0 to 4 times observed ice velocities, which are unaccompanied by corresponding ice stress variations. This renders it challenging to accurately predict all frontal ablation rate observations using the VM model and a fixed value of $\sigma_{max}$. The SR relation estimates that the ice stresses responsible for calving are a function of ice thickness and water depth. However, we find that seasonal and inter-annual changes in ice thickness and water depth are not large enough to account for the ice stresses that are likely driving the observed variability in frontal ablation rates. The decrease in observation-optimized parameters for the VM and SR models from temporally-distributed observations at Jakobshavn Isbrae and Illullip Sermia implies that near-terminus ice physically weakens during the summer at these glaciers; a phenomenon for which there is no supporting observational or theoretical evidence. Both the temporally-optimized VM and SR models over-estimate low frontal ablation rates observed during non-summer months while generally under-estimating high frontal ablation rates from summer months, which results in calving rate errors of more than 100 m $d^{-1}$ in the most extreme cases (Figure 3.6). These systematic errors suggest that the VM and SR models are not accurate over monthly or sub-monthly time scales at glaciers which experience large seasonal fluctuations in frontal ablation rate. One explanation for the exhibited model deficiencies is that important physical controls on frontal ablation are not accounted for in the current VM and SR calving formulas. Recent observations and numerical modeling show that ice mélange and submarine undercutting are important drivers of frontal ablation on seasonal time scales, that suppress calving in winter and enhancing calving during the summer runoff season (Todd and Christoffersen, 2014; Cassotto et al., 2015; Fried et al., 2018). Inclusion of

these processes in calving rate models may help reconcile over-estimates of fall-winter-spring frontal ablation rates and under-estimates of summer frontal ablation rates.

Alternatively, we invoke the possibility that the VM and SR models are accurate only over longer time scales in which observed frontal ablation rates are less variable. Indeed, recent work by Choi et al. (2018) shows that an ice flow model using the VM calving model can accurately simulate terminus position change on an annual scale. However, there is evidence that seasonal terminus variability plays an important role in the initiation of major glacier retreat and dynamic destabilization. Observations from West Greenland suggest that a lack of spring advance combined with an extended calving season, potentially as a result of early mélange clearing and warmer fjord water, triggered multi-year retreats at several marine-terminating glaciers in the region in 2003 (Howat et al., 2010). Similarly, the recent retreats of many marine-terminating glaciers in Alaska from stable topographic constrictions began in years when the glaciers did not undergo seasonal advances, also coinciding with above-normal summer sea surface temperatures (McNabb and Hock, 2014). Multi-year retreat also appears imminent at Kangerdlussuaq glacier in East Greenland following two seasons of weak wintertime mélange and expanded calving seasons (Bevan et al., 2019). Ice flow and calving models that do not account for seasonality in terminus dynamics may therefore miss important dynamic changes that affect long-term discharge projections.

### 4.2. Calving rate models vs positions models

Although our analysis does not permit a direct model inter-comparison between calving position models and calving rate models, we consider several lines of evidence that suggest calving position models will likely be more accurate than calving rate models when employed in prognostic ice sheet models of the Greenland Ice Sheet. Uncertainties associated with optimized HAF and CD calving models are within the resolution of many Greenland Ice Sheet-scale model runs. Given the correspondence between terminus position change, ice velocity, and ice flux (Howat et al., 2010; Moon et al., 2015), terminus positions modeled by the HAF and CD models that are accurate to within an ice sheet model grid cell therefore minimize ice discharge errors in model projections. Moreover, we expect model biases for calving position models to remain fairly consistent through time, given the low sensitivities of both spatially-optimized and temporally-optimized model configurations, as well as the

relatively narrow ranges of observation-optimized parameter values needed to account for terminus conditions over time. In comparison, calibrations of optimal parameters in the VM and SR models are not consistent over seasonal time scales, which may result in substantial frontal ablation rate biases persisting for at least a portion of every year at individual glaciers or possibly ice-sheet wide. Calving rate models therefore have two potentially large sources of model bias: The first arises at individual glaciers when the VM and SR models are spatially-optimized to yield median bias of 0 m $d^{-1}$across the ice sheet as a whole. Although many glaciers will have model biases close to 0 m $d^{-1}$, model biases on the order of 10 m $d^{-1}$ will inevitably exist at some glaciers. The second, and likely larger source of model bias stems from the considerable model uncertainties and model sensitivities associated with temporally-optimized VM and SR models. Fixed values for $\sigma_{max}$ and $\sigma_{th}$ cannot reliably account for frontal ablation rate variability over time at a single glacier and especially not at multiple glaciers over time without likely generating relatively large model biases at individual glaciers. When implemented in predictive ice sheet models, these calving rate model biases will accrue into potentially large glacier length change and mass flux errors. For example, if we consider a consistent calving rate bias of 10 m $d^{-1}$ that persists for four months out of the year at an individual glacier (with 0 m $d^{-1}$ bias during the other 8 months), the accumulated glacier length error after one year will be around 1.2 km, while after 20 years will be approximately 25 km. Given the likely prospect of accumulated glacier length errors, we recommend the use of position calving models over calving rate models for simulation of terminus dynamics in Greenland ice sheet models.

Our results for calving position models and calving rate models have important limitations. Using observational data to test calving position models, we are not able to quantify down-fjord terminus misfits. The literature suggests that this is primarily a concern for the CD model, which has been shown to produce unrealistic glacier advance through basal over-deepenings (Nick et al., 2010; Amundson, 2016). However, this erroneous behavior is only found using 1-D flowline models, so it remains unclear whether the incorporation of full horizontal stresses remedies such advances (as in Todd et al., 2018), or whether 2-D ice flow models with the CD calving model have yet to be applied to the same fjord and forcing scenarios that generated unrealistic terminus advance in the 1-D models. Recent testing of the CD calving model in 2-D ice flow models does not reveal unrealistic glacier advance (Otero

et al., 2017; Choi et al., 2018), but we recommend further evaluation using different mass balance forcings before application of the CD model to the entire ice sheet.

The timescale over which frontal ablation processes should be represented remains poorly understood, which complicates the formation and evaluation of calving rate parameterizations. Furthermore, ice sheet models run at time steps that vary from two weeks to one year (Bindschadler et al, 2013). Our evaluation of VM and SR models against observations from monthly or sub-monthly time scales therefore only has direct implications for the use of these calving models over corresponding time scales. Our results do not quantify the accuracy of the VM and SR models on annual time scales. Indeed, from our analysis it is possible that over-estimated ablation rates during non-summer months may partially compensate for under-estimated ablation rates during summer months. However, for ice sheet models that resolve outlet glacier dynamics on monthly or weekly timescales, our analysis provides strong evidence that calving rate models are not able to reliably simulate patterns of observed frontal ablation rates with high fidelity.

### 4.3. Recommendations for improved calving representation

Based upon the results of our evaluation of six calving models against spatially and temporally varying observations, we recommend the use of calving position models for use as boundary criteria in ice sheet models of the Greenland Ice Sheet. Of the calving position models we tested, the CD criterion with $d_w = 24\ m$ demonstrated more accurate simulation of observed terminus positions than the HAF and FAF calving models, and notably, reproduced observed extents of floating ice tongues. However, a lack of correspondence between expected crevasse water depths and calibrated $d_w$ values supports the notion that the CD model should be considered an effective heuristic approach that captures underlying ice stresses and not an exact physical representation of the calving process (Benn et al., 2007b). Other approaches to predicting terminus position that are formulated in terms of near-terminus ice dynamics, such as the von Mises stress (Aschwanden et al, in review), or accumulated ice damage (Krug et al., 2014), should be pursued and evaluated against the CD model.

Lastly, opportunities exist for improved calving rate formulations. Investigation of calving rate model performances over seasonal and inter-annual time scales reveals the

inability of the current VM and SR calving models to account for a wide range of observed frontal ablation rates with fixed model configurations. The addition of submarine melt and specific undercutting mechanisms may help reconcile the systematic under-prediction of summertime frontal ablation rates by increasing near-terminus tensile stresses. Although direct observations of submarine undercutting morphologies will likely remain sparse around Greenland, comprehensive observations of oceanic and fjord conditions by NASA's Oceans Melting Greenland program may enable inclusion of realistic submarine melt representation (e.g. Wood et al., 2018) in future frontal ablation parameterizations. The coupling of a calving criterion with realistic melt undercutting morphology has recently shown promise in a 3-D full stokes simulation of Store Glacier in West Greenland (Todd et al, 2018). Further observations of frontal ablation rates on varying time scales may constrain the precise physical parameters that control frontal ablation rates on time scales relevant to dynamic glacier changes and that are important to represent in prognostic ice sheet models of Greenland (Fried et al., 2018).

## 5. Conclusions

We find that the height above flotation (HAF), fraction above flotation (FAF), crevasse depth (CD), von Mises yield stress (VM), and stress relation (SR) calving models can be empirically calibrated to individual glaciers, at specific times, to reproduce terminus dynamics at 50 representative glaciers in Greenland with near-equal accuracy. However, when model free parameters are calibrated to optimal values that best encompass calving observations across the ice sheet and through time, we find varying model performances. The CD model with 24 m of water in crevasses ($d_w = 24$ m) reproduces observed terminus positions with high fidelity and outperforms the HAF and FAF models across spatial and temporal scales. Optimized VM and SR calving rate models simulate observed frontal ablation rates across 50 sample glaciers reasonably well, but struggle to reproduce seasonal and short-term variability that occurs over many years in observed frontal ablation rates using fixed model configurations. Our results point to the potential for current calving rate model biases to cause substantial glacier length and/or ice flux errors when employed in ice sheet models. Given the calving model formulas tested in this study, we therefore more strongly recommend the use of empirically-calibrated calving position models as opposed to calving rate models for use as boundary criteria within ice sheet models of Greenland.

In addition to model strengths, our observational approach to calving model calibration and evaluation reveals important model weaknesses that highlight opportunities to improve representation of frontal ablation processes. Despite the demonstrated accuracy of the CD model on both grounded and floating glaciers, we find several inconsistencies in the model's physical representation that point to opportunities for the development of new, stress-based calving position models. Systematic biases exhibited by calibrated calving rate models suggest that additional physical parameters should be incorporated into calving rate models if rate models seek to reproduce observations on monthly time scales. Incorporation of melt undercutting and ice mélange through the coupling of calving rate models to runoff and fjord conditions is likely essential for improved simulation of sub-annual frontal ablation rates, as has been shown in several process studies (Todd and Christoffersen, 2014; Robel, 2017; Todd et al., 2018). Improved observations of ocean temperatures and surface runoff are necessary to constrain the relationship between melt undercutting and calving in Greenland, and to

evaluate melt-driven frontal ablation models that were not tested here (Luckman et al., 2015; Slater et al., 2017).

## 6. References

Amundson, J. M., Fahnestock, M., Truffer, M., Brown, J., & Luthi, M. P. (2010). Ice melange dynamics and implications for terminus stability, Jakobshavn Isbræ, Greenland. *Journal of Geophysical Research, 115*, 1–12.

Amundson, J. M. (2016). A mass-flux perspective of the tidewater glacier cycle. *Journal of Glaciology, 62*(231), 82–93.

Aschwanden, A., Fahnestock, M. A., & Truffer, M. (2016). Complex Greenland outlet glacier flow captured. *Nature communications*, *7*, 10524.

Aschwanden, A., Fahnestock, M. A., Truffer, M., Brinkerhoff, D. J., Hock, R., Khroulev, C., Mottram, R., & Khan, S. A. (in review). Contribution of the Greenland Ice Sheet to sea-level over the next millennium.

Åström, J.A., Vallot, D., Schäfer, M., Welty, E.Z., O'Neel, S., Bartholomaus, T.C., Liu, Y., Riikilä, T.I., Zwinger, T., Timonen, J. & Moore, J.C. (2014). Termini of calving glaciers as self-organized critical systems. *Nature Geoscience*, *7*(12), 874.

Bartholomaus, T. C., Larsen, C. F., O'Neel, S., & West, M. E. (2012). Calving seismicity from iceberg–sea surface interactions. *Journal of Geophysical Research: Earth Surface*, *117*(F4).

Bartholomaus, T. C., Larsen, C. F., & O'Neel, S. (2013). Does calving matter? Evidence for significant submarine melt. *Earth and Planetary Science Letters, 380*, 21–30.

Bartholomaus, T.C., Stearns, L.A., Sutherland, D.A., Shroyer, E.L., Nash, J.D., Walker, R.T., Catania, G., Felikson, D., Carroll, D., Fried, M.J. & Noël, B.P. (2016). Contrasts in the response of adjacent fjords and glaciers to ice-sheet surface melt in West Greenland. *Annals of Glaciology*, *57*(73), 25-38.

Bassis, J. N., & Jacobs, S. (2013). Diverse calving patterns linked to glacier geometry. *Nature Geoscience*, *6*(10), 833–836.

Bassis, J. N., & Walker, C. C. (2012). Upper and lower limits on the stability of calving glaciers from the yield strength envelope of ice. *Proceedings of the Royal Society A: Mathematical, Physical and Engineering Sciences, 468*(2140), 913–931.

Benn, D. I., Hulton, N. R. J., & Mottram, R. H. (2007b). "Calving laws", "sliding laws" and the stability of tidewater glaciers. *Annals of Glaciology*, *46*(1996), 123–130.

Benn, D. I., Warren, C. R., & Mottram, R. H. (2007a). Calving processes and the dynamics of calving glaciers. *Earth-Science Reviews*, *82*(3–4), 143–179.

Benn, D. I., Cowton, T., Todd, J., & Luckman, A. (2017). Glacier calving in Greenland. *Current Climate Change Reports*, *3*(4), 282-290.

Bevan, S. L., Luckman, A. J., & Murray, T. (2012). Glacier dynamics over the last quarter of a century at Helheim, Kangerdlugssuaq and 14 other major Greenland outlet glaciers. *Cryosphere*, *6*(5), 923–937.

Bevan, S. L., Luckman, A. J., Benn, D. I., Cowton, T., & Todd, J. (2019). Warming of SE Greenland shelf waters in 2016 primes large glacier for runaway retreat. *The Cryosphere Discussions*. 1–16.

Bindschadler, R.A., Nowicki, S., Abe-Ouchi, A., Aschwanden, A., Choi, H., Fastook, J., Granzow, G., Greve, R., Gutowski, G., Herzfeld, U. and Jackson, C. (2013). Ice-sheet model sensitivities to environmental forcing and their use in projecting future sea level (the SeaRISE project). *Journal of Glaciology*, *59*(214), 195.

Cassotto, R., Fahnestock, M., Amundson, J. M., Truffer, M., & Joughin, I. (2015). Seasonal and interannual variations in ice melange and its impact on terminus stability, Jakobshavn Isbræ, Greenland. *Journal of Glaciology*, *61*(225), 76–88.

Catania, G.A., Stearns, L.A., Sutherland, D.A., Fried, M.J., Bartholomaus, T.C., Morlighem, M., Shroyer, E. & Nash, J. (2018). Geometric controls on tidewater glacier retreat in central western Greenland. *Journal of Geophysical Research: Earth Surface*, *123*(8), 2024-2038.

Chen, X., Zhang, X., Church, J.A., Watson, C.S., King, M.A., Monselesan, D., Legresy, B. and Harig, C. (2017). The increasing rate of global mean sea-level rise during 1993–2014. *Nature Climate Change*, *7*(7), p.492.

Choi, Y., Morlighem, M., Wood, M., & Bondzio, J. H. (2018). Comparison of four calving laws to model Greenland outlet glaciers, *Cryosphere*, 3735–3746.

Colgan, W., Rajaram, H., Abdalati, W., McCutchan, C., Mottram, R., Moussavi, M. S., & Grigsby, S. (2016). Glacier crevasses: Observations, models, and mass balance implications. *Reviews of Geophysics*, *54*(1), 119-161.

Cook, S., Rutt, I. C., Murray, T., Luckman, A., Zwinger, T., Selmes, N., Goldsack, A., & James, T. D. (2014). Modelling environmental influences on calving at Helheim Glacier in eastern Greenland. *Cryosphere*, *8*(3), 827–841.

Cook, S., Zwinger, T., Rutt, I. C., O'Neel, S., & Murray, T. (2012). Testing the effect of water in crevasses on a physically based calving model. *Annals of Glaciology*, *53*(60), 90–96.

Cowton, T. R., Sole, A. J., Nienow, P. W., Slater, D. A., & Christoffersen, P. (2018). Linear response of east Greenland's tidewater glaciers to ocean/atmosphere warming. *Proceedings of the National Academy of Sciences*, *115*(31), 7907–7912.

Csatho, B.M., Schenk, A.F., van der Veen, C.J., Babonis, G., Duncan, K., Rezvanbehbahani, S., Van Den Broeke, M.R., Simonsen, S.B., Nagarajan, S. & van Angelen, J.H. (2014). Laser altimetry reveals complex pattern of Greenland Ice Sheet dynamics. *Proceedings of the National Academy of Sciences*, *111*(52), 18478-18483.

Cuffey, K. M., & Paterson, W. S. B. (2010). *The physics of glaciers*. Academic Press.

Dieng, H. B., Cazenave, A., Meyssignac, B., & Ablain, M. (2017). New estimate of the current rate of sea level rise from a sea level budget approach. *Geophysical Research Letters*, *44*(8), 3744–3751.

Enderlin, E.M., & Bartholomaus, T.C. (in prep). Testing the Nye formulation for crevasse depths: implications for crevasse-depth calving models.

Enderlin, E. M., & Hamilton, G. S. (2014). Estimates of iceberg submarine melting from high-resolution digital elevation models: application to Sermilik Fjord, East Greenland. *Journal of Glaciology*, *60*(224), 1084-1092.

Enderlin, E. M., & Howat, I. M. (2013). Submarine melt rate estimates for floating termini of Greenland outlet glaciers (2000-2010). *Journal of Glaciology*, *59*(213), 67–75.

Enderlin, E. M., Howat, I. M., Jeong, S., Noh, M. J., Van Angelen, J. H., & Van Den Broeke, M. R. (2014). An improved mass budget for the Greenland ice sheet. *Geophysical Research Letters*, *41*(3), 866–872.

Enderlin, E. M., Hamilton, G. S., O'Neel, S., Bartholomaus, T. C., Morlighem, M., & Holt, J. W. (2016). An empirical approach for estimating stress-coupling lengths for marine-terminating glaciers. *Frontiers in Earth Science*, *4*, 104.

Falkner, K.K., Melling, H., Münchow, A.M., Box, J.E., Wohlleben, T., Johnson, H.L., Gudmandsen, P., Samelson, R., Copland, L., Steffen, K. & Rignot, E. (2011). Context for the recent massive Petermann Glacier calving event. *Eos, Transactions American Geophysical Union*, *92*(14), 117-118.

Fried, M. J., Catania, G. A., Bartholomaus, T. C., Duncan, D., Davis, M., Stearns, L. A., Nash, J., Shroyer, E., & Sutherland, D. (2015). Distributed subglacial discharge drives significant submarine melt at a Greenland tidewater glacier. *Geophysical Research Letters*, *42*(21), 9328–9336.

Fried, M. J., Catania, G. A., Stearns, L. A., Sutherland, D. A., Bartholomaus, T. C., Shroyer, E., & Nash, J. (2018). Reconciling drivers of seasonal terminus advance and retreat at thirteen central west Greenland tidewater glaciers. *Journal of Geophysical Research: Earth Surface*, 1–18.

Funk, A. P. K. H. M. (2006). Anisotropic damage mechanics for viscoelastic ice, *Continuum Mech. Thermodyn. 17*, 387–408.

Funk, T. H. I. M., Iken, A., Gogineni, S., & Truffer, M. (2002). Mechanisms of fast flow in Jakobshavn Isbrae , West Greenland : Part III . Measurements of ice deformation , temperature and cross-borehole conductivity in boreholes to the bedrock, *48*. *Journal of Glaciology*. 48(162).

Fürst, J. J., Goelzer, H., & Huybrechts, P. (2015). Ice-dynamic projections of the Greenland ice sheet in response to atmospheric and oceanic warming. *Cryosphere*, *9*(3), 1039–1062.

Goelzer, H., Nowicki, S., Edwards, T., Beckley, M., Abe-Ouchi, A., Aschwanden, A., Calov, R., Gagliardini, O., Gillet-Chaulet, F., Golledge, N.R. & Gregory, J. (2018). Design and results of the ice sheet model initialisation initMIP-Greenland: an ISMIP6 intercomparison. *The Cryosphere*, *12*(4), 1433-1460.

Haubner, K., Box, J.E., Schlegel, N.J., Larour, E.Y., Morlighem, M., Solgaard, A.M., Kjeldsen, K.K., Larsen, S.H., Rignot, E., Dupont, T.K. & Kjær, K.H. (2018). Simulating ice thickness and velocity evolution of Upernavik Isstrom 1849-2012 by forcing prescribed terminus positions in ISSM. *Cryosphere*, *12*(4), 1511-1522.

Howat, I. (2017). MEaSUREs Greenland ice velocity: Selected glacier site velocity maps from optical images, Version 2 [subsets: W69.95N, W70.55N, W70.90N, W71.25N,

W71.65N, W72.00N]. Boulder, Colorado USA. NASA National Snow and Ice Data Center Distributed Active Archive Center. https://dx.doi.org/10.5067/VM5Dz20MYF5C, [accessed October 2018].

Howat, I. M., & Eddy, A. (2012). Multi-decadal retreat of Greenland's marine-terminating glaciers. *Journal of Glaciology*, *57*(203), 389–396.

Howat, I. M., Negrete, A., & Smith, B. E. (2014). The Greenland Ice Mapping Project (GIMP) land classification and surface elevation data sets. *Cryosphere*, *8*(4), 1509–1518.

Howat, I. M., Box, J. E., Ahn, Y., Herrington, A., & McFadden, E. M. (2010). Seasonal variability in the dynamics of marine-terminating outlet glaciers in Greenland. *Journal of Glaciology*, *56*(198), 601–613.

Iken, A., K. Echelmeyer, W. Harrison & M. Funk (1993). Mechanisms of fast flow in Jakobshavns Isbrae , West Greenland : Part I . Measurements of temperature and water level in deep boreholes, *Journal of Glaciology*, (131).

James, T. D., Murray, T., Selmes, N., Scharrer, K., & O'Leary, M. (2014). Buoyant flexure and basal crevassing in dynamic mass loss at Helheim Glacier. *Nature Geoscience*, *7*(8), 593–596.

Jenkins, A. (2011). Convection-driven melting near the grounding lines of ice shelves and tidewater glaciers. *Journal of Physical Oceanography*, *41*(12), 2279-2294.

Joughin, I., Smith, B. E., Howat, I. M., Scambos, T., & Moon, T. (2010). Greenland flow variability from ice-sheet-wide velocity mapping, *56*(197), 415–430.

Kehrl, L. M., Joughin, I., Shean, D. E., Floricioiu, D., & Krieger, L. (2017). Seasonal and interannual variabilities in terminus position, glacier velocity, and surface elevation at Helheim and Kangerlussuaq Glaciers from 2008 to 2016. *Journal of Geophysical Research: Earth Surface*, *122*(9), 1635–1652.

Khazendar, A., Fenty, I.G., Carroll, D., Gardner, A., Lee, C.M., Fukumori, I., Wang, O., Zhang, H., Seroussi, H., Moller, D. & Noël, B.P. (2019). Interruption of two decades of Jakobshavn Isbrae acceleration and thinning as regional ocean cools. *Nature Geoscience*, 1.

King, M.D., Howat, I.M., Jeong, S., Noh, M.J., Wouters, B., Noël, B. & Broeke, M.R. (2018). Seasonal to decadal variability in ice discharge from the Greenland ice sheet. *The Cryosphere*, *12*(12), 3813-3825.

Krug, J., Weiss, J., Gagliardini, O., & Durand, G. (2014). Combining damage and fracture mechanics to model calving. *The Cryosphere*, *8*(6), 2101–2117.

Lea, J. M. (2018). The Google Earth Engine Digitisation Tool ( GEEDiT ) and the Margin change Quantification Tool ( MaQiT ) – simple tools for the rapid mapping and quantification of changing Earth surface margins, 551–561.

Levermann, A., Albrecht, T., Winkelmann, R., Martin, M. A., Haseloff, M., & Joughin, I. (2012). Kinematic first-order calving law implies potential for abrupt ice-shelf retreat. *Cryosphere*, *6*(2), 273–286.

Luckman, A., Benn, D. I., Cottier, F., Bevan, S., Nilsen, F., & Inall, M. (2015). Calving rates at tidewater glaciers vary strongly with ocean temperature. *Nature Communications*, *6*(October), 8566.

Lüthi, M., Funk, M., Iken, A., Gogineni, S., & Truffer, M. (2002). Mechanisms of fast flow in Jakobshavn Isbræ, West Greenland: Part III. Measurements of ice deformation, temperature and cross-borehole conductivity in boreholes to the bedrock. *Journal of Glaciology*, *48*(162), 369-385.

Martin, C.F., Krabill, W.B., Manizade, S.S., Russell, R.L., Sonntag, J.G., Swift, R.N., & Yungel, J.K. (2012). Airborne topographic mapper calibration procedures and accuracy assessment. NASA Technical Reports, Vol. 20120008479(NASA/TM-2012-215891, GSFC.TM.5893.2012).

McNabb, R. W., & Hock, R. (2014). Journal of Geophysical Research: Earth Surface Variations in Alaska tidewater glacier frontal ablation ,. *Journal of Geophysical Research: Earth Surface*, *119*(2), 153–167.

Mercenier, R., Lüthi, M. P., & Vieli, A. (2017). Calving relation for tidewater glaciers based on detailed stress field analysis. *The Cryosphere Discussions*, (September), 1–33.

Moon, T., Joughin, I., Smith, B., & Howat, I. (2012). 21st-Century Evolution of Greenland Outlet Glacier Velocities. *Science*, *336*(6081), 576–578.

Moon, T., Joughin, I., & Smith, B. (2015). Seasonal to multiyear variability of glacier surface velocity, terminus position, and sea ice/ice mélange in northwest Greenland. *Journal of Geophysical Research: Earth Surface*, 730–744.

Morlighem, M., Williams, C.N., Rignot, E., An, L., Arndt, J.E., Bamber, J.L., Catania, G., Chauché, N., Dowdeswell, J.A., Dorschel, B. & Fenty, I. (2017). BedMachine v3: Complete bed topography and ocean bathymetry mapping of Greenland from multibeam echo sounding combined with mass conservation. *Geophysical Research Letters*, *44*(21),11-051.

Morlighem, M., Bondzio, J., Seroussi, H., Rignot, E., Larour, E., Humbert, A., & Rebuffi, S. (2016). Modeling of Store Gletscher's calving dynamics, West Greenland, in response to ocean thermal forcing. *Geophysical Research Letters*, *43*(6), 2659–2666.

Morlighem, M., Wood, M., Seroussi, H., Choi, Y., & Rignot, E. (2019). Modeling the response of northwest Greenland to enhanced ocean thermal forcing and subglacial discharge. *The Cryosphere*, *13*(2), 723-734.

Mottram, R. H., & Benn, D. I. (2009). Testing crevasse-depth models: a field study at Breiðamerkurjökull, Iceland. *Journal of Glaciology*, *55*(192), 746-752.

Motyka, R. J., Dryer, W. P., Amundson, J., Truffer, M., & Fahnestock, M. (2013). Rapid submarine melting driven by subglacial discharge, LeConte Glacier, Alaska. *Geophysical Research Letters*, *40*(19), 5153-5158.

Murray, T., Scharrer, K., James, T.D., Dye, S.R., Hanna, E., Booth, A.D., Selmes, N., Luckman, A., Hughes, A.L.C., Cook, S. & Huybrechts, P. (2010). Ocean regulation hypothesis for glacier dynamics in southeast Greenland and implications for ice sheet mass changes. *Journal of Geophysical Research: Earth Surface*, *115*(F3).

Murray, T., Scharrer, K., Selmes, N., Booth, A.D., James, T.D., Bevan, S.L., Bradley, J., Cook, S., Llana, L.C., Drocourt, Y. & Dyke, L. (2015). Extensive retreat of Greenland tidewater glaciers, 2000–2010. *Arctic, antarctic, and alpine research*, *47*(3), 427-447.

Nick, F. M., Van Der Veen, C. J., Vieli, A., & Benn, D. I. (2010). A physically based calving model applied to marine outlet glaciers and implications for the glacier dynamics. *Journal of Glaciology*, *56*(199), 781–794.

Nick, F. M., Vieli, A., Howat, I. M., & Joughin, I. (2009). Large-scale changes in Greenland outlet glacier dynamics triggered at the terminus. *Nature Geoscience*, *2*(2), 110–114.

Noh, M. J., & Howat, I. M. (2015). Automated stereo-photogrammetric DEM generation at high latitudes: Surface Extraction with TIN-based Search-space Minimization (SETSM) validation and demonstration over glaciated regions. *GIScience & Remote Sensing*, *52*(2), 198-217.

Nye, J.F. 1955. Correspondence. Comments on Dr. Loewe's letter and notes on crevasses. *J. Glaciology*., 2(17), 512–514.

Nye, J.F. 1957. The distribution of stress and velocity in glaciers and ice-sheets. *Proc. R. Soc. London*, Ser. A, 239(1216), 113–133.

O'Leary, M., & Christoffersen, P. (2013). Calving on tidewater glaciers amplified by submarine frontal melting. *Cryosphere*, *7*(1).

Otero, J., Navarro, F. J., Martín, C., Cuadrado, M. L., & Corcuera, M. I. (2010). Three-dimensional modelling of calving processes on Johnsons Glacier , Three-dimensional modelling of calving processes on Johnsons glacier, Livingston Island , Antarctica, *Journal of Glaciology*, *56(196)*, 113–133.

Otero, J., Navarro, F. J., Lapazaran, J. J., Welty, E., Puczko, D., & Finkelnburg, R. (2017). Modeling the Controls on the Front Position of a Tidewater Glacier in Svalbard. *Frontiers in Earth Science*, *5*(April), 1–11.

Peano, D., Colleoni, F., Quiquet, A., & Masina, S. (2017). Ice flux evolution in fast flowing areas of the Greenland ice sheet over the 20th and 21st centuries. *Journal of Glaciology*, *63*(239), 499-513.

Petrovic, J. J. (2003). Review mechanical properties of ice and snow. *Journal of materials science*, *38*(1), 1-6.

Porter, C., Morin, P., Howat, I., Noh, M., Bates, B., Peterman, K., Keesey, S., Schlenk, M., Gardiner, J., Tomko, K., Willis, M., Kelleher, C., Cloutier, M., Husby, E., Foga, S., Nakamura., H., Platson, M., Wethington., M. Jr., Williamson, C., Bauer, G., Enos, J., Arnold, G., Kramer, W., Becker, P., Doshi. A., D'Souza, C., Cummens, P., Laurier, F., & Bojensen, M. (2018). ArcticDEM, https://doi.org/10.7910/DVN/OHHUKH. V1. [accessed 2018].

Pralong, A.: Ductile Crevassing, in: Glacier Science and Environmental Change, edited by: Knight, P. G., Blackwell Publishing, Oxford, 62 pp., 2006.

Rignot, E., Fenty, I., Xu, Y., Cai, C., Velicogna, I., Cofaigh, C.Ó., Dowdeswell, J.A., Weinrebe, W., Catania, G. & Duncan, D. (2016b). Bathymetry data reveal glaciers vulnerable to ice-ocean interaction in Uummannaq and Vaigat glacial fjords, west Greenland. *Geophysical Research Letters*, *43*(6), 2667-2674.

Rignot, E., Xu, Y., Menemenlis, D., Mouginot, J., Scheuchl, B., Li, X., Morlighem, M., Seroussi, H., den Broeke, M.V., Fenty, I. & Cai, C. (2016a). Modeling of ocean-induced ice melt rates of five west Greenland glaciers over the past two decades. *Geophysical Research Letters*, *43*(12), pp.6374-6382.

Rignot, E., Jacobs, S., Mouginot, J., & Scheuchl, B. (2013). Ice-Shelf Melting Around Antarctica, *Science. 1337* (July), 1334–1337.

Rignot, E., Koppes, M., & Velicogna, I. (2010). Rapid submarine melting of the calving faces of West Greenland glaciers. *Nature Geoscience*, *3*(3), 187–191.

Robel, A. A. (2017). Thinning sea ice weakens buttressing force of iceberg mélange and promotes calving. *Nature Communications*, *8*, 1–7.

Slater, D. A., Nienow, P. W., Goldberg, D. N., Cowton, T. R., & Sole, A. J. (2017). A model for tidewater glacier undercutting by submarine melting. *Geophysical Research Letters*, *44*(5), 2360–2368.

Schild, K. M., & Hamilton, G. S. (2013). Seasonal variations of outlet glacier terminus position in Greenland. *Journal of Glaciology*, *59*(216), 759-770.

Slater, D. A., Nienow, P. W., Goldberg, D. N., Cowton, T. R., & Sole, A. J. (2017). A model for tidewater glacier undercutting by submarine melting. *Geophysical Research Letters*, *44*(5), 2360-2368.

Slater, D. A., Straneo, F., Das, S. B., Richards, C. G., Wagner, T. J. W., & Nienow, P. W. (2018). Localized Plumes Drive Front-Wide Ocean Melting of A Greenlandic Tidewater Glacier. *Geophysical Research Letters*, *45*(22), 12-350.

Straneo, F., Sutherland, D.A., Holland, D., Gladish, C., Hamilton, G.S., Johnson, H.L., Rignot, E., Xu, Y. and Koppes, M. (2012). Characteristics of ocean waters reaching Greenland's glaciers. *Annals of Glaciology*, *53*(60), pp.202-210.

Todd, J., & Christoffersen, P. (2014). Are seasonal calving dynamics forced by buttressing from ice mélange or undercutting by melting? Outcomes from full-Stokes simulations of Store Glacier, West Greenland. *Cryosphere*, *8*(6), 2353–2365. Todd, J.,

Christoffersen, P., Zwinger, T., Råback, P., Chauché, N., Benn, D., Luckman, A., Ryan, J., Toberg, N., Slater, D. and Hubbard, A. (2018). A full-Stokes 3-D calving model applied to a large Greenlandic glacier. *Journal of Geophysical Research: Earth Surface*, *123*(3), pp.410-432.

Van den Broeke, M.R., Enderlin, E.M., Howat, I.M., Kuipers Munneke, P., Noël, B.P., Jan Van De Berg, W., Van Meijgaard, E. and Wouters, B. (2016). On the recent contribution of the Greenland ice sheet to sea level change. *The Cryosphere*, *10*(5), 1933-1946.

van der Veen, C. J. (1996). Tidewater calving. *Journal of Glaciology*, *42*(141), 375–385.

van der Veen, C. J. (2013). Fundamentals of Glacier Dynamics, CRC Press.

Veitch, S. A., & Nettles, M. (2012). Spatial and temporal variations in Greenland glacial-earthquake activity, *Journal of Geophysical Research.* 1993 – 2010, *117*.

Vieli, A., Funk, M., & Blatter, H. (2001). Flow dynamics of tidewater glaciers: A numerical modelling approach. *Journal of Glaciology*, *47*, 595–606.

Vieli, A., & Nick, F. M. (2011). Understanding and Modelling Rapid Dynamic Changes of Tidewater Outlet Glaciers: Issues and Implications. *Surveys in Geophysics*, *32*(4–5), 437–458.

Wagner, T. J. W., Straneo, F., Richards, C. G., Slater, D. A., Stevens, L. A., Das, S. B., & Singh, H. (2018). Large spatial variations in the frontal mass budget of a Greenland tidewater glacier. *The Cryosphere Discussions*, *2018* (July), 1–19.

Wood, M., Mouginot, J., & Rignot, E. (2018). Ocean-Induced Melt Triggers Glacier Retreat in Northwest Greenland, *Geophysical Research Letters, 45, 8334–8342.*.

Xu, Y., Rignot, E., Fenty, I., Menemenlis, D., & Flexas, M. M. (2013). Subaqueous melting of Store Glacier , west Greenland from three-dimensional , high-resolution numerical modeling and ocean observations, *Geophysical Research Letters. 40*, 4648–4653.